8-2013

Multiscale Modeling of Toxoplasma gondii

Adam Michael Sullivan
asulli17@utk.edu

To the Graduate Council:

I am submitting herewith a dissertation written by Adam Michael Sullivan entitled "Multiscale Modeling of Toxoplasma gondii." I have examined the final electronic copy of this dissertation for form and content and recommend that it be accepted in partial fulfillment of the requirements for the degree of Doctor of Philosophy, with a major in Biomedical Engineering.

Xiaopeng Zhao, Major Professor

We have read this dissertation and recommend its acceptance:

MIchael A. Gilchrist, Chunlei Su, William R. Hamel

Accepted for the Council:

Carolyn R. Hodges

Vice Provost and Dean of the Graduate School

(Original signatures are on file with official student records.)

8-2013

Multiscale Modeling of Toxoplasma gondii

Adam Michael Sullivan
asulli17@utk.edu

To the Graduate Council:

I am submitting herewith a dissertation written by Adam Michael Sullivan entitled "Multiscale Modeling of Toxoplasma gondii." I have examined the final electronic copy of this dissertation for form and content and recommend that it be accepted in partial fulfillment of the requirements for the degree of Doctor of Philosophy, with a major in Biomedical Engineering.

Xiaopeng Zhao, Major Professor

We have read this dissertation and recommend its acceptance:

MIchael A. Gilchrist, Chunlei Su, William R. Hamel

Accepted for the Council:
Carolyn R. Hodges

Vice Provost and Dean of the Graduate School

(Original signatures are on file with official student records.)

Multiscale Modeling of Toxoplasma gondii

A Dissertation

Presented for the

Doctor of Philosophy

Degree

The University of Tennessee, Knoxville

Adam Michael Sullivan

August 2013

To my wife Jessica and beautiful daughter, Ava.

Acknowledgements

I would like to thank Dr. Xiaopeng Zhao for the guidance and friendship as I journeyed through the maturity of becoming a full-time researcher. I would like to equally thank Dr. Michael Gilchrist for teaching me the pursuit of perfection in research.

I am thankful to my committee members Dr. Chunlei Su and Dr. William Hamel. I am also thankful to the many members of the National Institute of Mathematical and Biological Synthesis, along with their financial support for my research.

Lord, take me where you want me to go, let me meet who You want me to meet, tell me what you want me to say, and keep me out of Your way. Amen. Father Mychal Judge

Abstract

Toxoplasma gondii is a parasite capable of causing diseases such as encephalitis, birth defects, and abortion to infected hosts that uses a very unique life cycle to manipulate the cell and immune systems. To investigate the mechanics of how the parasite spreads within hosts, several related models are developed to study the within-host dynamics of *Toxoplasma gondii*. Understanding the complicated methods of how the parasite grows, dies, invades, replicates, and evades the host immune response is the critical aim of this independent research. The processes of acute and chronic infection are studied independently to understand the dynamics of the infection at both stages, followed by an attempt to understand the entire duration of the infection through one system. Finally, a probabilistic rule-based model is simulated within a 3D mesh representation of a mouse brain to visualize the infection spreading during the acute and chronic phase. The results presented shed light onto the effects of the immune response, cyst volume growth, and the dependence of multiple stages in the dissemination of the parasite within a host.

Contents

List of Tables

List of Figures

Chapter 1

Introduction

Toxoplasma gondii is a potentially deadly parasite capable of infecting mammals and birds. The parasite is unique in that it uses the cat to divide sexually while using all hosts to divide asexually. The most common means of transmission is ingestion of oocysts released into the environment by felidae species, the parasites definitive host, or by ingestion of the persistent bradyzoite cysts in animal tissues. Following ingestion, parasites penetrate the host's intestinal epithelium and undergo a developmental switch to the rapidly replicating tachyzoite parasite stage, which is then disseminated systemically. Disseminated toxoplasmosis is likely the result of a few parasites that successfully penetrate across the intestinal barrier, evade mucosal immunity including effector activity of recruited inflammatory monocytes[103, 51, 49]. The parasites are capable of converting between the stages of tachyzoites and bradyzoites [47].

Each stage of parasite triggers a different immune response where the immune response fights back against tachyzoite infected cells while bradyzoites trigger an immune response unique from that of tachyzoites. From *in vivo* experiments, mice that are in the chronic state who become immunosuppressed will exhibit an increased invasion rate of parasites into host cells, indicating that the chronic state is regulated by the immune response [60].

Toxoplasma gondii is an important parasite because of the role it plays in human health. The chronic infection rate of the parasite ranges from 20% in the US to 50% and higher in other countries [4]. Although the chronic infection state is asymptomatic, hosts who develop an immune deficiency are capable of triggering a very large secondary acute attack that is capable of serious illness or death. Additionally, becoming infected with parasites while bearing a child in utero can cause serious birth defects to the unborn child, up to and including abortion [4].

It is interesting to note that *T. gondii* plays a role in the behavior of human health and behavior. Parasites that have infected the brain are capable of causing behavioral changes in the host. The behavioral change of infected mice has been observed in *in vivo* experiments that observed parasite-cat interactions [14, 71]. When mice are infected with *T. gondii*, the mice are attracted to the cats urine, thus altering the brain function of the mice [91, 134].

In this work, we aim to develop a better understanding of *T. gondii* because of the role it plays in human health. By understanding how the parasite behaves using mathematical and computational methods, we hope to be able to address some of the lingering questions regarding *T. gondii* not explored experimentally.

The within-host dynamics of the parasite can be understood by breaking the processes into separate parts before attempting to combine the processes into a single effort. A model is developed to understand the biological processes that are undertook while a host experiences an acute infection. Additionally, a model to describe the later chronic infection of the host is developed to understand the biology while the host typically exhibits very few symptoms caused by the parasite.

Once these two models are developed, the acute and chronic stages are combined into a single mathematical model to describe the transition from the acute stage to the chronic stage. This model provides insights into the role of the immune response for the duration of the infection. Finally, the model developed for both stages is transformed into a rule-based probabilistic algorithm to model the infection within the brain. The computational model provides data output during the simulation

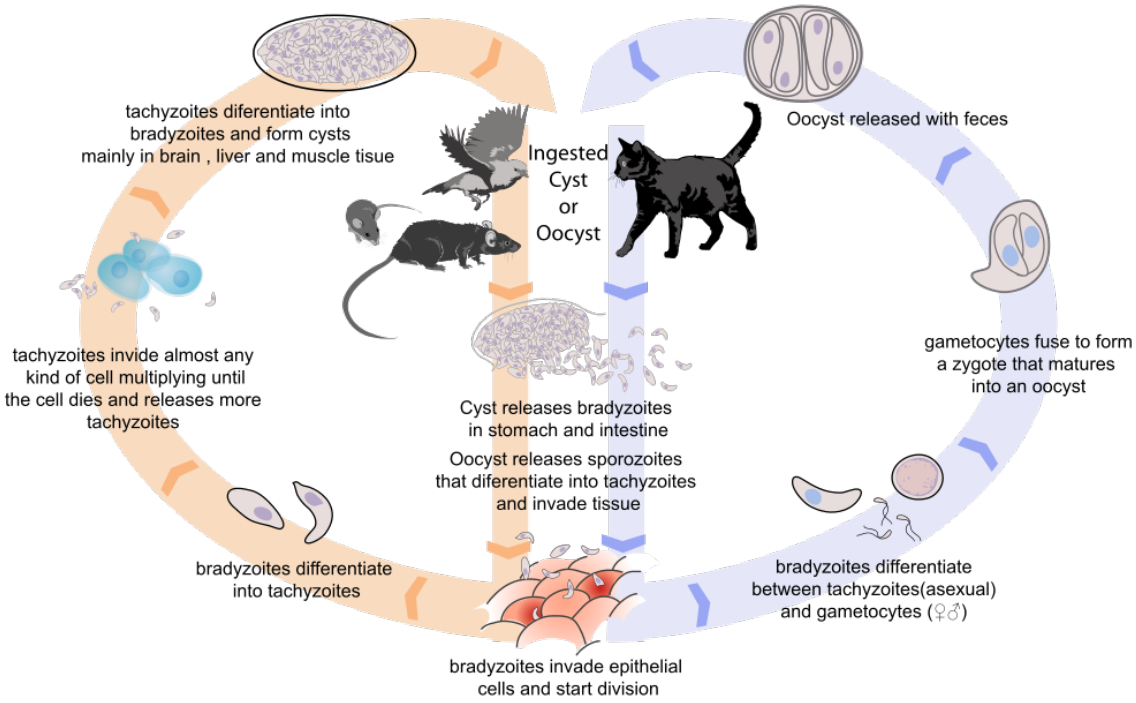

Figure 1.1: Life Cycle of *Toxoplasma gondii* from [136].

along with the functionality of outputting the infection as 3D representations of the brain.

The acute infection process is important to study because the most harm can be done to the host during this stage. The acute infection features a large number of parasites replicating and disseminating very quickly, causing a very rapid immune response. If unchecked, the parasites could replicate in such a way to cause the host to die. Additionally, an immune response can cause the host to develop immune pathology. Thus, understanding the acute infection is very important.

Our hypothesis of the acute infection is that it may be possible for the parasites to undergo various stages during the invasion process of the life-cycle. The testing of the effects of the multiple stages of the parasitic infection and immune response is performed by analyzing 16 different nested models to determine which model best fits the available experimental data. Understanding these stages allows us to develop a better understanding of the life cycle. Additionally, the overall fit of the model to

the data gives evidence that the model is supported by the data, and thus allowing us to claim support for the assumptions made in the model.

The answer to those questions are supported by a model that we are the first to build using commonly understood models from cellular dynamic systems. The ODE model we developed is unique in its application to *T. gondii*.

The chronic infection period of a *Toxoplasma gondii* infection typically is asymptomatic to the host. However, there are interesting biological questions to be answered during this process because a resurgence of the infection can be caused by a compromised immune response. Thus, understanding how the immune response and the dissemination of parasites occurs during the chronic state is important. There are two questions that can be answered by modeling the chronic state of the parasitic infection: 1) Do the assumptions we make in our model support the experimental data for cyst-volume distributions, and 2) Can we differentiate the growth, death, and bursting functions for the cyst distributions?

The assumptions we made about our model appear to be supported by the data because the model was able to capture the behavior of the data. However, we could not differentiate between the growth, death, and bursting functions, instead opting for functions that combined the effects of each growth/removal function due to the lack of identifiability for some parameters. It may be possible to differentiate between these parameters given data at different time points in the infection.

The model that was developed is a model adapted from research done with other biological phenomena, typically with regard to age of an individual and the biomass of an individual (for example, *Daphnia*). However, we are the first to adapt this model to *T. gondii* and examine different growth/death functions within the context of within-host dynamics, specially examining the volume growth of cysts infected with bradyzoites.

After examining the acute and chronic stages of the infection, the combined effects of these two different stages acting on a single system are evaluated. Initially, the intention of the within-host dynamics model was to explore the equilibrium points of

the infection. Interestingly, the model demonstrated that the infection was capable of persisting either with or without the immune response, despite the widely understood belief that immuncompromised mice cannot survive an invasion of *T gondii*. Thus, it may be possible for a nonvirulent parasite strain to invade an immunocompromised host and the host will not die.

The within-host model attempts to link the parasitic invasion dynamics with the host-cell population dynamics during chronic and acute stages of infection. This complicated model is the first of its kind to be applied to *T. gondii* with regards to incorporating stage-conversion, parasite invasion, and host-cell infection. The introduction of a two-class system for bradyzoites is unique for classifying bradyzoites as either cells ready to convert back to tachyzoites after invasion or bradyzoites that will form cysts. This model answers novel questions regarding the 3 different fixed points of the system and effect the immune response has (for example, one of the diseased fixed points is absent of immune response, indicating that the parasite can persist at low enough levels that the immune response is not needed to keep the parasites in equilibrium).

Following the development of the the within-host dynamics model, there still remained questions regarding the findings found in the chronic infection model. The acute and within-host models do not account for size of infected host cells and there was not a way to validate the chronic infection results. Thus, a discrete-time rule-based simulation was created in C++ to simulate the interactions between cells, parasites, and the immune response. This rule-based model was developed as a tool to further understand the mechanisms of *T. gondii* infection.

The development of a cellular automata model for modeling and visualizing the parasitic infection in a brain novel in that we are the first to develop this type of model for this type of parasitic infection. Other models have been developed using tumors to visualize replication of tumor cells that we borrowed some principles in modeling from, although our model is significantly different because of the nature of

the infection. The model allows us to display numerical and visual results to aid in our discussions with biologists.

The model is capable of outputting the relative sizes of infected cysts, the variables measured in the chronic infection model. In the course of developing this model, we hypothesized three different assumptions for the method in which the parasites replicate within cysts. By running the simulation using each of the three different replication mechanisms, we develop support for the models generated during the chronic infection.

As demonstrated, the research presented here is unique and novel, especially in the application of models to the problem of *T. gondii*. The models answer novel questions regarding the impact of the immune response, the role of replication within cysts, the role of differentiated stages of parasites and immune response on the acute infection state, and the exploration of the specific method of replication within the cysts.

Chapter 2

Literature Survey

2.1 Toxoplasma gondii

Toxoplasma gondii is a parasitoid that infects up to 20% of the US population [4]. While the parasite does not typically cause death when an individual becomes infected, those with deficient immune systems and unborn children may die from contracting the parasite. The effect it has on humans makes this an important parasite to study and monitor.

The between-host dynamics is a complicated cycle that exists between mammals and birds. The parasite uses the feline to reproduce sexually. When the cat becomes infected, it sheds oocysts, which contaminates the environment. These oocysts can be ingested by mammals and birds which then become infected with the parasite[47]. Eating another organism that is infected can also infect the secondary host. Studying the effects of asexual reproduction in secondary hosts has been performed biologically, however, much work can still be done on reproducing the results of the life-cycle of the parasite mathematically [77].

The within-host life cycle of a parasite starts out as a tachyzoite, which reproduces asexually very quickly. The tachyzoites infect host cells, where they feed off of the nutrients in the host to reproduce. Once the parasite replicate several times,

the parasites will burst from the host cell and continue to infect other host cells. Sometimes, the parasites will convert to a new stage of *Toxoplasma* known as a bradyzoite. These parasites replicate very slowly and will eventually form a cyst within a host cell (most often in muscle and brain tissue). The cysts are filled with a few up to thousands of bradyzoites, and can remain alive for days even after a host has died. The consumption of undercooked meat is one way to release a bradyzoite cyst [4].

Once the host cell containing bradyzoite bursts, each bradyzoite can then re-infect new host cells, thus completing the life cycle within the host. Tachyzoites are rapidly dividing and responsible for the symptoms of acute infection whereas the slowly replicating bradyzoites are located within tissue cysts, which protect the parasite from the host immune system and make it inaccessible to drugs [47]. The differentiation of tachyzoites into bradyzoites is a response to the onset of protective immunity whereas the dormant bradyzoites are able to reconvert into tachyzoites to cause fatal infection. Therefore, stage conversion between tachyzoites and bradyzoites plays a pivotal role in the pathogenesis, transmission, persistence, and reactivation of the disease.

Thy lytic cycle of *T. gondii* consist of the parasite entering a host cell, replicating, and then lysing out of the host cell when the replicated parasites egress from the host cell [19]. A parasitophorous vacuole (PV) is formed to allow parasites to replicate within the host cell, while external stress factors may trigger egress of the parasites. During early infection, the PV acts as a barrier to keep the parasites within the host cell and to reduce the effect of the immune response [94]. Typically, the rapid, cytolytic release of parasites lyses the host cell as the parasites break through the parasitophorous vacuole membrane, the host cytoplasm, and finally the plasmalemma [19]. *T. gondii* is unique from the viral lytic cycle in that the parasite is very active during invasion (compared to bacteria and viruses) where the motility and unique shape provide a very quick and precise invasion into a host cell [29]. Further, while the parasite is undergoing the lytic cycle, it is possible for the parasite to spontaneously

convert from tachyzoite to bradyzoite or vice-versa. A variety of external stress factors, including an IFN-γ mediated immune response, are responsible for the stage-conversion from tachyzoite to bradyzoite during early infection [121]. Eventually, bradyzoites make up the majority of parasites found within a host.

There are qualitative observations of the size distributions of cysts found in brain tissue. Isolated tissue cysts in several experiments ranged from 20 μm to 70 μm in diameter [94]. The number of cysts found in the brains of an mouse infected with the HIF strain of *T. gondii* ranged from 290 to 1380 and ranged from 10 to 70 μm [15]. In that experiment, 80% of cysts were solitary while the other 20 % were found in groups of two or larger. Further, it has been reported that as much as 92% of the brain regions contained cysts in one such experiment [15]. The timing of the steady-state typically occurs around 2 months while the number of cysts per brain (and the copies of parasite DNA) peaked near 40-60 days [110].

Few comprehensive experiments regarding the size distribution of cysts during chronic infection exist. There is anticipation of new experimental designs to more effectively quantify the numbers and sizes of cysts in the brain through high-throughput epifluorescence microscopy where the counting method is fully automated [8]. Other attempts to quantify the number of cysts using photon emission imaging to observe concentrations of cysts give insights into the total cyst load in the mouse, but not the relative sizes of the cysts [40].

The steady-state dynamics of the parasite is controlled by the immune response. Cysts can evade the immune response through the thick cyst walls [94]. T-cells and IFN-γ are the main players in maintaining tachyzoite replication and preventing reactivation of infection [129]. Reactivation occurs when the immune response is compromised and does not suppress cyst development, causing a release of parasites into the brain. It is unknown how frequently reactivation occurs, and experimental evidence was not able to detect enough reactivation events to predict the frequency of reactivation [131]. Reactivation by means of a secondary infection, as in the case of a mouse previously infected with a non-virulent strain and later infected with a

highly-virulent strain, is not a common occurrence, and thus a previous infection provides some immunity from new infections [57].

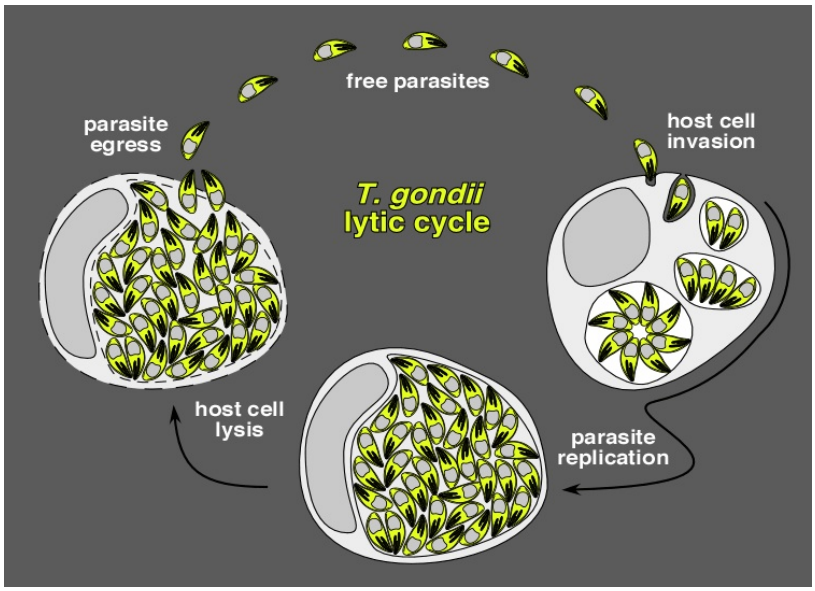

Figure 2.1: Lytic Cycle of *Toxoplasma gondii* from [65].

There are differing opinions on the underlying processes that occur during chronic infection of an infected host. It is unknown whether cysts form and remain in a cyst form for nearly the life of host or if there is a constant dynamic process of bursting cysts combined with invasion that has no net change in cyst formations in the host. A well-developed model will be able to provide some insight into the question of cyst formation. By developing a strong data-driven model for cyst formation, it may be possible to develop better immunological treatment plans for immunocompromised patients infected with chronic *Toxoplasma gondii*.

2.2 Modeling Techniques

In developing the mathematical frameworks for the different stages of the infection (acute, chronic, and combined-stages), it became apparent that there is a need to develop different techniques for each method. Therefore, each of the different

modeling techniques are surveyed below. In addition, some of the technical needs of applying these models to data are presented as well.

2.2.1 ODE Modeling

The phenomenon of parasites invading hosts and healthy host cells has been modeled using mathematical models quite heavily [111, 70, 10]. The techniques of modeling parasites on the within-host scale follow very similar parallels to the modeling techniques of between-host modeling.

One of the best parallels to parasitic within-host modeling occurs through virus dynamics modeling. For example, a model could be developed between target cells, productively infected cells, uninfected cells that are refractory to infections, free virus, and IFN to describe the flu[109]. In that paper, the authors use the above state variables to find parameter matches to match experimental data. Another model developed where target cells, free virions, and infected target cells are modeled as a system [31, 21, 62].

To best illustrate the method of linearization of nonlinear ODE systems, the classical paper by Anderson and May is reviewed [11]. In Anderson and May, they propose a model for infectious disease modeling by introducing a dynamic "N", the total population. The host population was previously taken to be constant. They begin by introducing the diversity of agents causing disease. There are two different types: microparasites and macroparasites. Microparasites reproduce at much higher rates within the host, and immunity is more likely for those who survive the initial infection. The duration of the infection is typically short. Macroparasites have much longer generation times and direct multiplication is non-existant or very slow. Macroparasitic infections tend to be more of a persistent nature.

In the studies of mice populations studied by the researchers, mice are introduced at a certain rate (A), in units of mice introduced per day. The total number of mice, $N = X + Y + Z$, is not assumed to be some independently-set constant, but is set

by the dynamics of the infection. The mortality rate of this model is given by b, the natural mortality rate. Trivially, the disease-free population would equilibrate to $N* = A/b$. The modeling equations then become:

$$\begin{aligned}
\frac{dX}{dt} &= A - bX - \beta XY + \gamma Z \\
\frac{dY}{dt} &= \beta XY - (b + \alpha + \nu)Y \\
\frac{dZ}{dt} &= \nu Y - (\gamma + b)Z \\
\frac{dN}{dt} &= A - bN - \alpha Y
\end{aligned}$$

where b is the natural death rate, γ is the immunity loss rate, α is the disease death rate, ν is the infected recovery rate, and β is the transmission term which incorporates interactions between susceptible and infected individuals [11].

The equations have a stable equilibrium solution if:

$$A/b > (\alpha + b + \nu)/\beta$$

This type of linearization about a fixed point is surveyed heavily in Kot [96]. If this condition is not met, the disease dies out and the population equilibrates to the disease free stability point $N*$. If the inequality is satisfied, the total population is then depressed to:

$$N^* = \frac{A + D(\alpha + b + \nu)/\beta}{b + D}$$

where $D = \alpha/[1 + \nu/(b + \gamma)]$.

These modeling equations were fit to data observed in experiments carried out by researchers on the effects of mice. Too large of an α makes it impossible for a disease to persist (since it is killing to population too rapidly to spread effectively) while a small α would have very little effect on N^*. The author suggests that diseases caused by microparasites are more likely to persist within, and cause severe reduction

of, host populations with high birth (or immigration) rates; this phenomenon derives essentially from the high inflow of susceptibles [11].

When considering a birth rate rather than an introduction rate, the system merely change to:

$$\begin{aligned}
\frac{dX}{dt} &= a(X+Y+Z) - bX - \beta XY + \gamma Z \\
\frac{dY}{dt} &= \beta XY - (b+\alpha+\nu)Y \\
\frac{dZ}{dt} &= \nu Y - (\gamma+b)Z \\
\frac{dN}{dt} &= (a-b)N - \alpha Y
\end{aligned}$$

And a natural intrinsic growth rate is given to be $r = a - b$. The parameter stability inequality is then given by:

$$\alpha > r\left[1 + \frac{\nu}{b+\gamma}\right]$$

If this equation holds true, then the equilibrium point of the population is:

$$\frac{\alpha(\alpha+b+\nu)}{\beta[\alpha - r(1+\nu/(b+\gamma))]}$$

If the inequality is not true, the disease will grow exponentially (but necessarily less that r):

$$\rho = [B^2 - (b+\gamma)(\alpha - r) + r\nu]^{\frac{1}{2}} - B$$

where $B = \frac{1}{2}(\alpha + b + \nu + \gamma - r)$. The asymptotic prevalence of the infection would be $y = Y/N \to (r-\rho)/\alpha$.

If N is less than some value $N_T = (\alpha + b + \nu)/\beta$ then initially Y will decrease and X will increase exponentially at rate r. However, once X exceeds N_T, then Y will increase, and the system will either converge to N^* or N will grow at the slower rate ρ, depending whether the inequality is satisfied.

If the disease death rate is much higher than the intrinsic disease-free growth rate, it is likely that prevalence settles to be small as to give a high probability for stochastic fade out. Epidemics can occur when $r > \alpha$ if the disease does not regulate the host population but merely slows its growth rate slightly. Infections of short duration which induce lasting immunity will tend to exhibit epidemic patterns [11].

Of particular interest is the way they handle vertical transmission. A fraction of births from the infected class are also infected. Therefore, the threshold host population (minimum population for successful introduction of the disease) is given by $(\alpha + b + \nu - f\alpha)/\beta$. The threshold is zero if $f\alpha > \alpha + b + \nu$.

Other work has been done to represent R_0, the reproductive number for *Toxoplasma gondii*. In this mouse transmission system, we assume that R_0, the reproductive number of disease, is a function of several biological phenomena. To model this, we assume that R_0 can be modeled for a system using a modified R_0 operator:

$$R_0 = \frac{\beta}{d + \alpha} \tag{2.1}$$

where β is the predation rate of infected mice, d is the natural death rate of the mice, and α is the parasitic-caused death rate of the mice caused by virulence [43, 41]. This assumes that the next-generation operator for the diseased cat-mouse system would be a function of cat predation on mice and virulence of the mice. The modeling of cats and mice in a coupled ODE system has been observed before where the reproductive number R_0 has been calculated before [92, 93].

2.2.2 Partial Differential Equation Modeling

Some of the partial differential equations related to age modeling of a population correspond to the volumetric growth of parasite densities and cell sizes. For example, the McKendrick-von Foerster PDE [96, 88] can be written as

$$\frac{\partial n}{\partial t} + \frac{\partial n}{\partial a} = -\mu(a, t)n \tag{2.2}$$

where n is the density of all females and $\mu(a,t)$ is a death rate that depends on both the age of the individual and the time. The boundary condition for such a partial differential equation is

$$n(0,t) = \int_0^{\omega} n(a,t)m(a,t)da \tag{2.3}$$

and an initial condition $n(a,0) = n_0(a)$.

The above system models the population density as a function of time and age. However, in the world of parasites, the volume of a parasite-containing cell is of interest during the chronic infection period. Therefore, it is important to take into account the time of infection and the volume of the cyst in determining the parasite-cell densities. Therefore, the model from Sinko [119] is presented

$$\frac{\partial n(t,a,m)}{\partial t} + \frac{\partial n(t,a,m)}{\partial a} + \frac{\partial}{\partial a}[g(t,a,m)n(t,a,m)] = -D(t,a,m)n(t,a,m) \tag{2.4}$$

where n(t,a,m) is the density function, $g(t,a,m)$ is the growth rate that depends on time, age, and biomass, and $D(t,a,m)$ is the removal function that depends on time, age, and biomass. The boundary conditions specify that $a(a,m) = n(0,a,m)$ and $B(t,m) = n(t,0,m)$ where $a(a,m)$ is the number of animals at age a and mass m that initially exist at time $t = 0$, and $B(t,m)$ is the number of newborn animals with mass m that exist at time t. Oldfield refined this system to accurately describe the growth of a population with respect to just time and mass [108].

One instance where the size distribution of the population is of importance is in the study of *Daphnia*, which are small planktonic crustaceans that live in the water and grow with time and size [54]. In the *Daphnia* model, the population of *Daphnia* interact with a predator which reduces the population. The density of the population depends on the number of individuals and their sizes for a given population.

2.2.3 Optimization and Analyzing Results

Part of the topic of this research is to introduce and analyze different sets of data and derive parameters for models. For example, in the chronic infection model, an experiment was performed to collect cyst-size measurements from 4 mice after 4 months of infection. These measurements are then used in analyzing the parameters of the model. Additionally, in the acute infection section of this research, data is used to fit the model for both the parasite counts and the immune response interaction.

To perform model selection of different models fitted to the same data set, several different methods were used. One such technique that we used involved the maximum likelihood function [27, 18, 132]. The likelihood function is typically defined as

$$\mathcal{L} = \prod p(d_i|\lambda) \tag{2.5}$$

where $p(d_i|\lambda)$ is the probability of observing the data point i given the parameters λ. This function is easier to handle numerically when the negative log-likelihood is considered [22]. The log-likelihood function can be written as

$$L = \sum p(d_i|\lambda) \tag{2.6}$$

Developing the proper probability functions that are used in the minimization technique is important in being able to find the global minima of the negative log-likelihood function [22]. The probability function for a density function with no error term can be assumed to be

$$p(d_i|\lambda) = \frac{f(d_i)}{\int f(s)ds} \tag{2.7}$$

However, if we assume that there is noise in the observation, we can make a probability function based on the observation and prediction of a given function. For example, if the function one wants to estimate the probability for is $y\ a + bx$, the measurement could really be estimated as $y_{obs}\ a + bx + \epsilon$, where ϵ is some noise term

[69]. By assuming the noise term is distributed normally about 0 with some standard deviation, $N(0, \sigma)$, one can derive the probability of a normally distributed function to be

$$p(d_i|\lambda) = \frac{1}{2\pi\sigma} \exp(\frac{(y_{obs} - y_{pred})^2}{2\sigma^2} \tag{2.8}$$

Using a minimization technique to minimize the negative log-likelihood becomes easy to do numerically for optimization problems that are not highly nonlinear. To test this, a minimization technique in Mathematica, R, or Matlab can be used to find the minima of the objective function. It is important to be certain the the global minima is the value returned from the minimization technique. To insure this, the minimization algorithm should be performed many times using different initial conditions and possibly different searching techniques (Nelder-Mead, Simulated Annealing, Differential Evolution, etc).

The best way to compare nested models that are evaluated using the maximum likelihood is to use the AIC approach. The AIC allows one to compare models using the negative log likelihood as a reward while the number of parameters as a penalty [23]. For the AIC, method of minimizing the negative log likelihood while minimizing the number of parameters predicts the best model fit to existing data [7]. The AIC value is calculated as

$$\text{AIC} = -2\log(\mathcal{L}) + 2n_p \tag{2.9}$$

where n_p is the number of parameters in the particular nested model. It is important to use nested models and the same data set when attempting to compare AIC's of different models. The definition of $\Delta\text{AIC}_i = \text{AIC}_i$ - AIC_{best} gives a way to compare models. The criteria for accepting a model based on the ΔAIC is: 0-2 best evidence of acceptance, 3-7 less evidence of best selection, 10+ almost no evidence of a fit supported by the model and data [27].

2.2.4 Bayesian Statistics

In the case of highly nonlinear problems, it may be very difficult to find a global minima to the negative log likelihood objective function [22]. In the case where finding the global through different searching routines is not possible, it may be necessary to resort to bayesian statistics and the Markov Chain Monte Carlo routine to find the parameters that best fit the model.

The Markov Chain Monte Carlo method that is best suited for the problems presented in this research is the Metropolis-Hastings algorithm. The best parameters are found by searching around the parameter space with a random walk. Some prior information regarding the distribution of the parameters is assumed and the posterior distributions of the parameters are found.

More specifically, the Metropolis-Hastings routine first is given an initial parameter, x_t. A new distribution of parameters is generated based on the current parameter choice [114]. For our model, the objective function is a chi-squared distribution which is denoted by f. Further, the distribution of parameters is a conditional density of q. Thus, x_{t+1} takes on the new value with probability $\min\left(\frac{f(Y_t)}{f(x_t)}\frac{q(x_t|Y_t)}{q(Y_t|x_t)}, 1\right)$. Otherwise, x_{t+1} retains the value of x_t.

In this algorithm, it is required to specify an effective "step size" that represents the variance of normal distribution of each parameter that we are searching for.

Once the MCMC generates a sufficient number of samples, it is necessary to thin the sample to reduce any autocorrelation in the individual parameter spaces. Once thinning is performed, the mean of the individual parameter samples is the parameter estimate.

To evaluate the "fit" of the model, the DIC is used to find best fitting nested model (deviance information criteria) [17]. The deviance is defined as $D(\lambda) = -2\log(p(y|\lambda)) + C$. The expectation of the deviance is $\bar{D} = E^{\lambda}[D(\theta)]$. The effective

number of parameters is found as $p_D = \bar{D} - D(\bar{\lambda})$[17]. Therefore, the DIC is

$$DIC = p_D + \bar{D} \tag{2.10}$$

Chapter 3

Acute Infection ODE Model

3.1 Introduction

Toxoplasma gondii is an obligate intracellular protozoal parasite and the causative agent of toxoplasmosis. The most common means of transmission is ingestion of oocysts released into the environment by felidae species, the parasite's definitive host, or by ingestion of the persistent bradyzoite cysts in animal tissues. Following ingestion, parasites penetrate the host's intestinal epithelium and undergo a developmental switch to the rapidly replicating tachyzoite parasite stage, which is then disseminated systemically. Disseminated toxoplasmosis is likely the result of a few parasites that successfully penetrate across the intestinal barrier and evade mucosal immunity, including effector activity of recruited inflammatory monocytes[103, 51, 49].

The lytic cycle of *T. gondii* begins with the invasion of a host cell by the free parasites followed by their replication within a parasitiphorous vacuole(PV) inside the cell. Eventually the parasites trigger the lysis of the cell by a yet undefined process at which time parasites are released from the PV into the intracellular space[82, 12, 19]. Unlike the majority of intracellular pathogens, *T. gondii* actively invades host cells instead of relying on phagocytosis for entry [46]. This, in part, allows the parasites to invade and replicate within virtually any type of vertebrate host cell. During invasion

of a host cell, the parasite forms a nascent PV that is largely segregated from host endocytic and exocytic pathways [102, 101, 126, 32].

An IFN-γ-dependent cell mediated immune response is critical for the control of *T. gondii* infection (reviewed in [39]). In immunocompromised IFN-γ deficient mice, *T. gondii* replication is relatively unrestrained and results in rampant parasite replication, dissemination, and the host death [128]. IFN-γ production by NK cells, and CD4+ and CD8+ T cells is driven in large part by early IL-12 production by innate immune cells including dendritic cells [98], macrophages [113], inflammatory monocytes [103] and neutrophils [20]. IFN-γ- subsequently activates inflammatory monocytes [103, 49, 50, 112] and other hematopoietic cells as wells as non-hematopoietic cells [139] to suppress or kill intracellular parasites through a variety of cell autonomous immune effectors (reviewed in [97]).

Even in immune-competent hosts, parasites likely encounter an initial environment permissive to dissemination and replication within host cells early in the infection. However, as time progresses, the IFN-γ-dependent innate, and eventually the cell-mediated immune response becomes mobilized mobilized, leading to the clearance of the majority of parasites. Nevertheless, some tachyzoites survive their acute stage of infection and convert to the slow growing and more immuno-resistant bradyzoite developmental stage. Bradyzoites are encased in cysts created within an infected host cell. In the presence of an acute immune response, bradyzoites are relatively quiescent and can persist for long periods, months or years. However, in the absence of IFN-γ or effective cell mediated immunity, the bradyzoites can convert back to tachyzoites causing re-initiation of active infection and severe pathology and death [115, 61, 127].

It is clear that IFN-γ production, IFN-γ-dependent activation of cell autonomous antimicrobial mechanisms in host cells, and IFN-γ-dependent cell mediated immunity are clear determinants in whether *T. gondii* survives and replicates or is killed following the invasion of a host cells during infection. Because of the complex interactions between IFN-γ levels and *T. gondii* densities, we develop a compartmental model to

describe the relationship between the initial onset of infection and the host IFN-γ-dependent immune response.

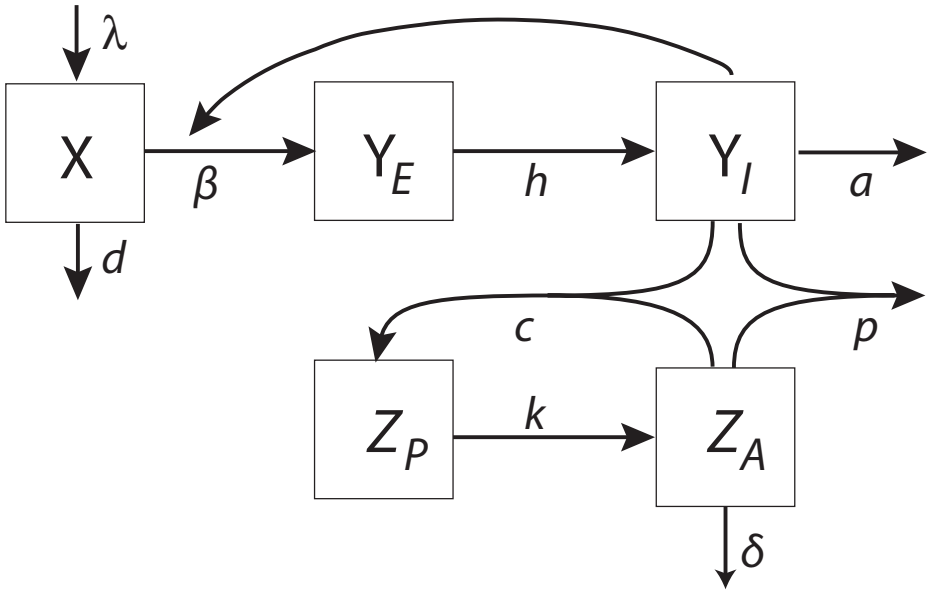

Figure 3.1: Representation of our Compartmental model for *T. gondii* infection. X represents susceptible host cells, Y_E represents the host cells that are exposed to parasites, Y_I represents the infected host cells that have been activated, Z_P represents the primed immune response, and Z_A represents the activated immune response. See Table 3.1 and below for the definitions of all model parameters.

3.2 Model and Method

3.2.1 Model Description

We first present a framework to describe the tachyzoite lytic cycle that dominates the early, acute infection process. For simplicity, we assume that acute infection is dominated by tachyzoites and, therefore, neglect bradyzoites in our framework. The dynamics of inter-conversion between tachyzoites and bradyzoites have been empirically studied in [123] while the growth of bradyzoites in chronic stage has been studied in [125]. Figure 6.1 shows a compartmental description of the model. The state variables include the densities of uninfected cells, X; the densities of exposed

host cells (Y_E) which are not yet capable of producing parasites, which acts as a delay for the infected host cells because cells of this type cannot cause new infections; the densities of infected host cells (Y_I) that are capable of causing an increased immune response and larger numbers of tachyzoites within a PV; the densities of primed immune cells (Z_P) which acts as a delay class in the immune response by limiting the removal of infected cells[95]; and the densities of activated immune cells capable of causing removal of infected cells (Z_A).

We assume uninfected cells are generated at a constant rate λ and assume a constant background cell removal of d. In the absence of an infection, the population dynamics of host cells are given by $\dot{X} = \lambda - dX$. Under this simple population dynamics model, the number of uninfected cells stably converges to the equilibrium $X_0 = \lambda/d$. We assume that during acute infection the number of infected host cells is only a small fraction of the total host cells, which implies that any change in X is small, remaining essentially constant throughout the acute infection phase, that is $X = X_0$. This assumption is applied throughout the rest of the paper.

The generation of exposed cells Y_E is proportional to the product of the abundance in healthy host cells and the abundance of infected host cells: $\beta X Y_I$. The rate constant, β is a composite parameter describing the efficacy of the invasion process and depends on the rate at which the parasites find uninfected cells, the rate of parasite entry, and the probability of successful invasion. The exposed cells convert to the infectious category at a rate: hY_E. The average life time of infected cells is $1/a$. We consider a simple model of immune response: Z_P, which consists of a primed response and Z_A, activated response. We assume the activated immune immune cells encounter and attack infected cells according to a mass action model with rate constant p and that these interactions also recruit primed immune cells with efficiency c/p such tha the net rate of primed cell recruitment is $cY_I Z_A$. The primed immune cells Z_P become activated at constant rate k. The average life time of activated immune cells is $1/\delta$. Parameters are described in Table 3.1.

Table 3.1: Definitions of model parameters

Parameter	Definition
β	transmission rate of infection (1/cell-day)
h	conversion rate of cells infected with early-type parasites to cells with infection-causing parasites (1/day)
a	natural death rate of cells infected with parasites (1/day)
p	removal of parasites caused by interaction with immune response (10mL)/(day-ng)
c	recruitment rate of early-type immune response caused by interaction with parasites (1/(cell-day))
k	conversion of early-type immune response to immune response capable of removing parasites (1/day)
δ	decay rate of killing-capable immune response (1/day)

Combining the above processes leads to the following system of equations:

$$Y_E' = \beta X_0 Y_I - hY_E \tag{3.1}$$

$$Y_I' = hY_E - pY_I Z_A - aY_I \tag{3.2}$$

$$Z_P' = cY_I Z_A - kZ_P \tag{3.3}$$

$$Z_A' = kZ_P - \delta Z_A \tag{3.4}$$

The system possesses two equilibria. The first is a disease free equilibrium (DFE):

$$(Y_E^*, Y_I^*, Z_P^*, Z_A^*) = (0, 0, 0, 0). \tag{3.5}$$

The second is an endemic equilibrium:

$$(Y_I^*, Y_E^*, Z_P^*, Z_A^*) = \left(\frac{\beta X_0 \delta}{ch}, \frac{\delta}{c}, \frac{\delta(\beta X_0 - a)}{kp}, \frac{(\beta X_0 - a)}{p} \right) \tag{3.6}$$

which is biologically infeasible if $\beta X_0 < a$.

Using the next generation matrix approach [42], we can show that the basic reproduction number is

$$R_0 = \frac{\beta X_0}{a}. \tag{3.7}$$

It follows that the disease free equation will be stable if and only if $R_0 < 1$. From the Routh-Hurwitz stability criterion [89], we can show that the endemic equilibrium is stable if $R_0 > 1$.

Next, we will present the simplifications of the system (3.1)-(5.2) under different quasi steady-state assumptions.

Primed immune response Z_P in quasi steady state:

Here we assume the primed immune response is in quasi steady state, that is, $Z_P = cY_I Z_A/k$. The biological assumption here is that we assume that there is not a secondary class of immune response triggered by infected cells. It follows that the system (3.1)-(5.2) can be reduced to:

$$\begin{aligned} Y_E' &= \beta X_0 Y_I - hY_E & (3.8)\\ Y_I' &= hY_E - pY_I Z_A - aY_I & (3.9)\\ Z_A' &= cY_I Z_A - \delta Z_A & (3.10) \end{aligned}$$

Exposed cells Y_E in quasi steady state:

Assume the exposed cells are in quasi steady state, that is, $Y_E = \beta X_0 Y_I/h$. This model tests the notion that the invasion process is very fast and a secondary state of infected cells does not help capture the dynamics of the infection process. It follows

that the system (3.1)-(5.2) can be reduced to:

$$Y_I' = \beta X_0 Y_I - p Y_I Z_A - a Y_I \quad (3.11)$$

$$Z_P' = c Y_I Z_A - k Z_P \quad (3.12)$$

$$Z_A' = k Z_P - \delta Z_A \quad (3.13)$$

Primed Immune Response and Exposed Cells Z_P and Y_E in quasi steady state:

Assume the primed immune response and the exposed cells are in quasi steady state, that is, $Z_P = cY_I Z_A/k$ and $Y_E = \beta X_0 Y_I/h$. This model assumes that a single class of infected cells and immune response captures the dynamics of the infection. It follows that the system (3.1)-(5.2) can be reduced to:

$$Y_I' = \beta X_0 Y_I - p Y_I Z_A - a Y_I \quad (3.14)$$

$$Z_A' = c Y_I Z_A - \delta Z_A \quad (3.15)$$

3.2.2 Bayesian Parameter Fitting

Mordue et al. measured evolution of parasite load and immune response during acute toxoplasmosis in mice [104] and we fit our models to this data in order to estimate parameters of the models using a Markov Chain Monte Carlo (MCMC) Bayesian approach [100, 67]. IFN-γ levels are taken from blood samples and average parasite counts taken from peritoneum tissue cultures.

In their experiments, Mordue et al. [104] started to collect the parasite and immune data two days after infection since the parasite load and the immune level are at very low levels in the first two days. In simulations of the models, we shift the time coordinate of the models so that the initials conditions of the models correspond to data at day 2 in the experiments.

To develop biologically sound assumptions of our model, care is taken in formulating the initial conditions for the systems. Generally, we assume that at the start of the experimental collection, there are only populations of one type of parasite-infected host cells and one type of immune response present. This biological assumption leads to the following initial conditions for each nested model:

- **Full Model:** We set $Y_I(0) = 0$ and $Z_A(0) = 0$, and estimate $Y_E(0)$ and $Z_P(0)$ from parameter fitting.
- Z_P **in quasi steady state:** We set $Y_I(0) = 0$ and estimate $Y_E(0)$ and $Z_A(0)$ from parameter fitting.
- Y_E **in quasi steady state:** We set $Z_A(0) = 0$ and estimate $Y_I(0)$ and $Z_P(0)$ from parameter fitting.
- Z_P **and** Y_E **in quasi steady state:** We estimate $Y_I(0)$ and $Z_A(0)$ from parameter fitting.

Burkart [26] developed a MCMC routine in Mathematica [138]. The routine uses the MCMC Metropolis-Hastings method for performing a random walk in the parameter space that will reflect samples from the posterior [74]. We implement the models in Mathematica and adopt Burkart's package for parameter fitting. We assume that our objective likelihood function is distributed as a normal distribution. The variances that are used are found by estimating the measurement errors from the experimental data.

In this parameter fitting algorithm, it is required to specify an effective step size that represents the variance of normal distribution of each parameter that we are searching for. To find a good starting estimate for this distribution, we ran 4 sets of 40,000 MCMC samples and recorded the parameter choices. We then used the variances from these initial runs designate our step size variance.

We used an adaptive MCMC algorithm where at every every 10,000 samples, the algorithm would evaluate the average acceptance rate for those 10,000 samples and

adjust the scaling to get the average acceptance rate between 0.1 and 0.4 [13].We run the simulations for 300,000 samples for each of the four models. We thin the 300,000 samples by 1,000 to reduce autocorrelation between the samples [140]. We used the means, standard deviations, and confidence intervals of the posterior samples as our summary statistics.

While our models are based on the number of infected host cells, experiments lack this resolution to measure both free parasites and those that are in cells together in a single parasite count using extracts from homogenized tissues [104]. Since Y_E represents an early exposed stage, we assume each Y_E cell contains only one tachyzoite. Let us denote the expected number of tachyzoites an infected host cell by n_t. Then, we estimate the total number of parasites found in a homogenized tissue sample as follows:

$$P = Y_E + n_t Y_I. \tag{3.16}$$

In the following simulations, we estimate the model parameters when $n_t = 1$, 2, 4, and 8, respectively.

The 300,000 MCMC samples of the model are compiled with the first 10% considered as burn-in samples. The Deviance Information Criterion (DIC) is often used as the model selection technique in MCMC simulations [122, 16]. DIC can be regarded as a generalization of the Akaike information criterion (AIC) and the Bayesian information criterion (BIC).

3.3 Results

According to the DIC, the experimental data are bested described by the full model with $n_t = 4$. Table 3.2 shows the DIC values for each model.

The mean values of the parameter posteriors (parameter estimates) and the 95% posterior probabilities for the best model with $n_t = 4$ are presented in Table 3.3. The

Table 3.2: DIC Values for Each Model. The full model with $n_t = 4$ is the best performing model.

n_t	Full Model	Y_E in QSS	Z_P in QSS	Y_E & Z_P in QSS
1	82.6	130.9	167.5	163.1
2	90.5	114.5	125.1	144.7
4	53.2	106.2	88.2	136.7
8	57.4	112.4	106.1	137.8

QSS stands for quasi steady state.

fits of the alternative sub-models to experimental data when $n_t = 4$ are shown in Figure 3.2.

Table 3.3: Parameter Estimates andPosterior Probability Intervals for the Best Model; see DIC in Table 3.2.

Parameter	Estimate	95% Posterior Probability Interval
βX_0	0.56	$\{0.40, 0.77\}$
h	2.67	$\{2.35, 3.09\}$
p	0.23	$\{0.21, 0.30\}$
a	0.60	$\{0.34, 0.93\}$
c	0.33	$\{0.16, 0.51\}$
k	0.79	$\{0.69, 0.98\}$
δ	2.25	$\{0.99, 3.62\}$
Y_0	13.63	$\{8.63, 19.07\}$
Z_0	0.08	$\{0.02, 0.16\}$

3.4 Discussion and Conclusion

The model presented here was created to model the biological phenomenon associated with immune response dynamics in acute *T.gondii* infection. Linear stability analyses were performed to examine the stability of the model's two fixed points: disease-free equilibrium and an endemic equilibrium with continuing immune response. The full ODE model and sub models derived from it were fitted to parasite density and IFN-γ data for infected mice previously reported in [104]. Parameters of the model were

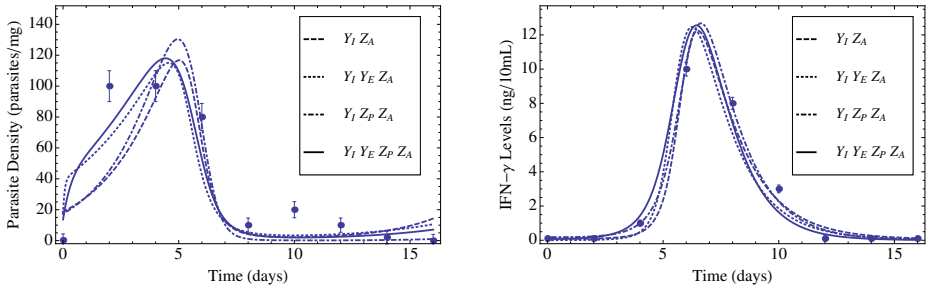

Figure 3.2: Illustrations of model fits to parasite and immunological data. The solid line is the $Y_E Y_I Z_P Z_A$ model, the dashed line $(--)$ is the $Y_I Z_A$ model, the dotted line is the $Y_E Y_I Z_A$ model $(\cdots)$ and the dash-dotted is the $Y_I Z_P Z_A$ $(- \cdot -\cdot)$ model.

estimated based on the posterior samples of a Bayesian MCMC algorithm and models were compared using the DIC.

Using the DIC as a model selection method in Table 3.2, we find that the full model has the greatest support is the model that includes all 4 state variables, Y_E,Y_I, Z_P, and Z_A with $n_t = 4$. It is worth noting that the DIC penalizes models for each of their parameters, yet the model selection criteria supports the model with the greatest number of parameters. The data and model-selection technique suggests that the best description of the phenomenon is one in which the presence of primed immune response and exposed cells infected with parasites play a prominent role. If a primed immune response or exposed cells infected with parasites played a very small role in the phenomenon, the model selection would have supported one of the sub models. Thus, we conclude that the data indicates that a delay in the immune response and parasitic invasion make an important contribution to the overall dynamics of invasion. The second best model contains the same 4 state variables with $n_t = 8$. As a qualitative conclusion, the plots of the models over the data observations in Figure 3.2 all have similar shapes and fits.

The patterns exhibited by the parasite density-immune response interaction shows a strong correlation between the two. Our results indicate that if the parasites enter at a low level and don't replicate very quickly, the immune response would not be triggered. However, a virulent strain of parasite, or large numbers of parasites, would

trigger a very large transient immune response. The data used in this paper supports the biological phenomenon observed because the original experiment tested larger doses of parasites and more virulent strains than the Type II strain of parasite used for this model [104].

In future work, having raw data would allow for more accurate predictions of the parasite counts because more realistic error distributions could be found. Additionally, we have assumed that the healthy cell count, X, remains constant throughout the infection. Having estimates for the reduction in the healthy cell counts would provide a third state variable to use for parameter estimation, thus providing a more accurate estimate of the parameters. We also believe that introducing other immune response indicators such as CD-8+ counts, IL-12, or other immune response measurements could add complexity but more accuracy to the model.

Visually inspection of the plots of the models over the data, the model without any delay and the model with a delay in the parasite activation both present a small level in the parasite levels. We associate this regeneration of parasites as a low level of parasites that biologically would not trigger a second infection. In general, the parameter fitting algorithm provides a realistic representation of the parameters used in the different models. One advantage of using the MCMC approach over a global minima search routine is that the spread of the parameter estimates are described by the variability of the posterior distributions.

The goal of building this model was to determine whether there is evidence to support an exposed cell class or a primed immune response class in dealing with the life-cycle of the *Toxoplasma gondii* parasite. Based on the model-selection analysis, there is support for the less-active classes of parasite-infected cells and immune response. Developing an understanding of these secondary classes will aid in understanding a variety of issues pertaining to *T. gondii* including mortality, strain virulence, and stage conversion factors, among others.

Chapter 4

Chronic Infection PDE Model

4.1 Model and Method

4.1.1 Sampling and Estimating the Volume of *T. gondii* Cysts from the Brain Tissue of Chronically Infected Mice

T. gondii has three predominant clonal genotypes (types I, II, and III) [37, 64, 73]. Type II constitutes a majority of clinical cases of toxoplasmosis and asymptomatic infections in humans in North America and Europe[6, 37, 73]. Therefore, a type II strain, ME49, was used for this study. Female Swiss-Webster mice (Taconic, Germantown, NY) were infected intraperitoneally with 10 cysts of the ME49 strain as previously described [84]. Six months later, the brain of each of four mice was triturated in 1 ml of PBS [130]. Four to six aliquots (20 ml each) of each brain suspension were applied to microscopic examination using a Nikon Eclipse 90i microscope and a photograph was taken on each *T. gondii* cyst detected at x400 magnification with a Nikon DS-Ri1 digital camera. Photographs of 50-56 cysts from each brain, a total of 213 from four mice, were recorded (see Figure 4.1 for a typical photograph of a cyst). Due to the fact that a small proportion of cysts appear

to be more ellipsoid than spherical, we measured the diameter of each cyst from two different angles using NIS Elements BR analysis 3.2 software. The measured diameters of each cyst are shown in Figure 4.2.

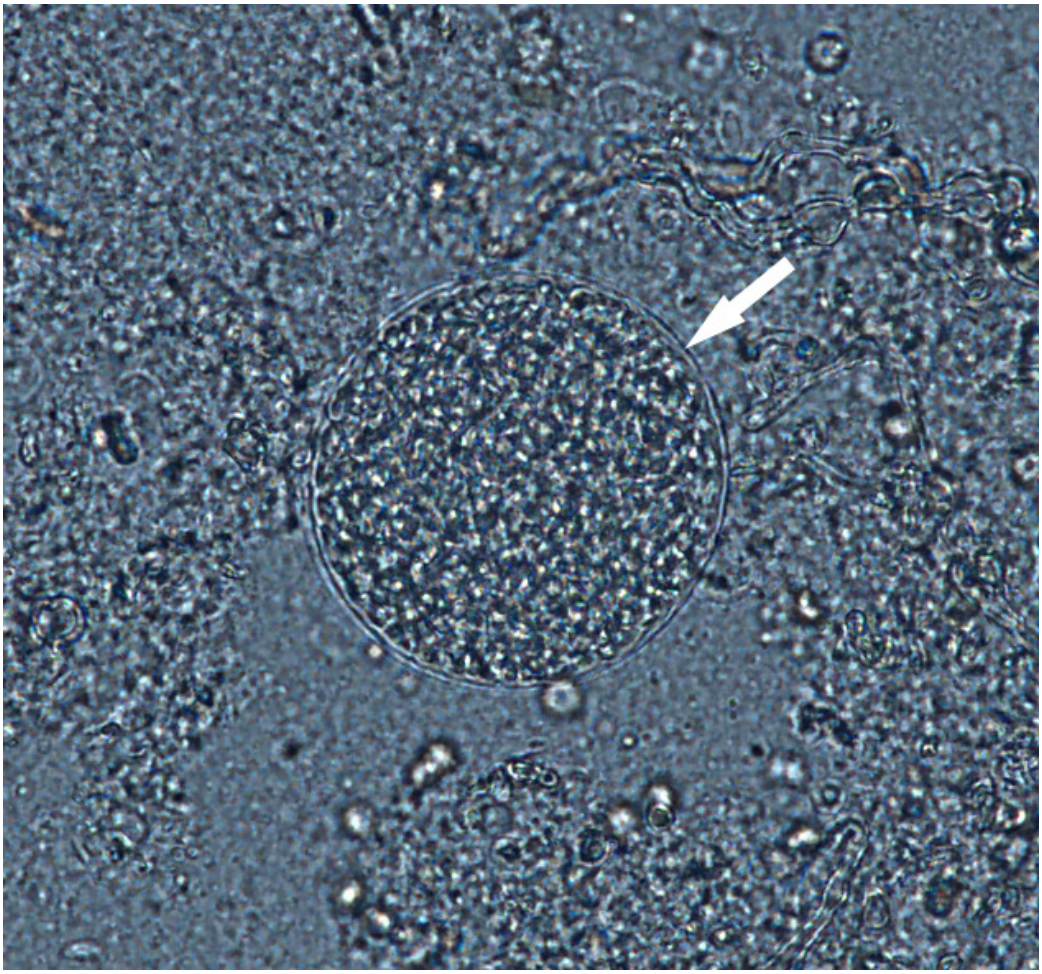

Figure 4.1: Example of photograph of a cyst from our experiment. Most of the cysts observed took on similar nearly circular cross section projections.

4.1.2 Modeling Cyst Formation & Growth

There have been several attempts to understand the biology of *Toxoplasma gondii* infection through mathematical modeling [123, 77], however, none of these previous efforts have tried to model the growth and distribution of cysts as a function of their volume. Because in this study we are solely interested in the distribution of

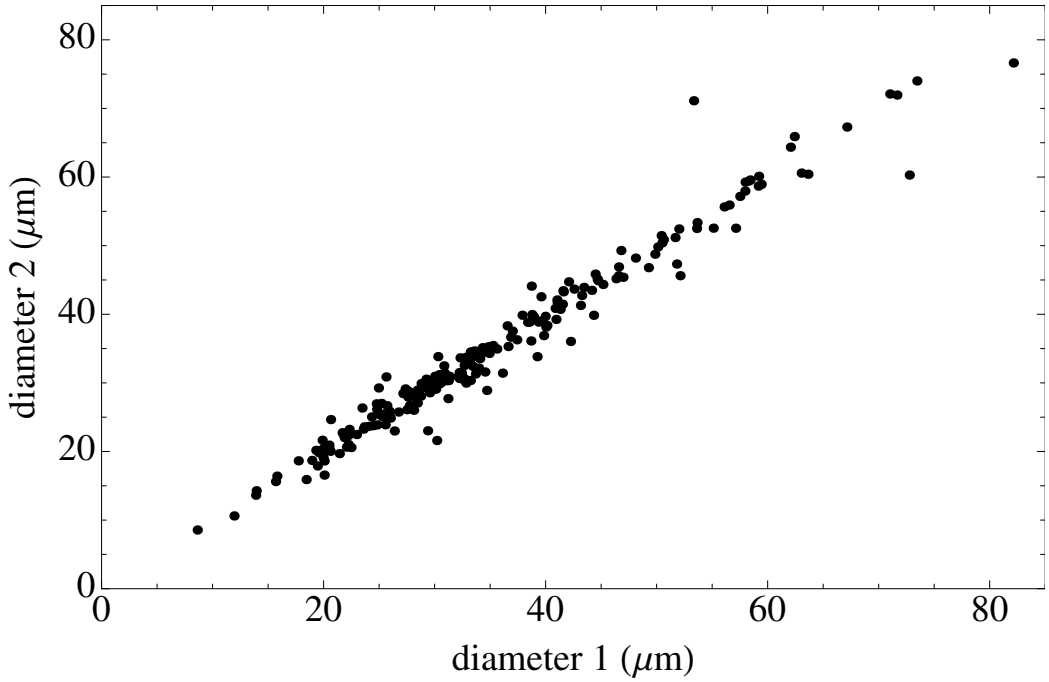

Figure 4.2: The diameter d_1 measurements vs the d_2 measurements. The relationship between each diameter is shown to indicate that the projected cysts were nearly spherical.

cyst volumes, we can avoid having to explicitly model population of free bradyzoites, tachyzoites, and uninfected target cells and, instead, simply assume new cysts are being formed at some rate $B(t)$. See Figure 4.3 for a schematic of the within-host system and Table 4.1 for definitions of the functions used in our model. Biologically $B(t)$ represents the rate at which uninfected target cells become infected by free parasites and begin forming cysts intracellularly. Following [119], we model the growth of these cysts using a partial differential equation structured by both time and cyst volume. Specifically,

$$\frac{\partial Y(t,v)}{\partial t} + \frac{\partial}{\partial v}\left(g(v)Y(t,v)\right) = -r(v)Y(t,v) \tag{4.1}$$

where $Y(t,v)$ is the density of bradyzoite cysts of volume v at time t, $g(v)$ is cyst growth rate, i.e.the rate at which bradyzoites replicate within a cyst, and $r(v)$ is the cyst removal rate, i.e. the sum of the rate at which encysted cells are

either cleared by the immune response or through natural cyst bursting. Although these two cyst removal processes differ in that bursting ultimately leads to the production of new cysts while immune response clearance does not, their effects on the relative distribution of cysts as a function of volume are indistinguishable and, hence, combined in Equation 4.1. Biologically, both $g(v)$ and $r(v)$ likely vary with the immune response state of the host. However, since we are focusing on the steady state of the system where the immune response state of the host is constant, we do not explicitly model this dependency. Because cyst volumes are finite, we restrict ourselves to growth functions where $\lim_{v\to\infty} g(v) = 0$ such that a finite, maximum cyst size $v_{\max}$ exists. Assuming that all new cysts have the initial volume v_0, based on our definition of $B(t)$ as the rate at which new cysts are formed, according to [34] the boundary condition for Equation 4.1 satisfies the equality,

$$B(t) = g(v_0)Y(t, v_0). \tag{4.2}$$

4.1.3 Steady-state Solution

Although Equation 4.1 can be explicitly solved as a function of time (e.g. see [28]), here we focus solely on the steady state solution. We begin by presenting the general solution and then later assume specific functional forms for cyst growth $g(v)$ and removal $r(v)$.

Letting $\hat{Y}$ represent the absolute distribution of cyst volumes at steady state at which point, by definition, $\frac{\partial Y}{\partial t}|_{\hat{Y}} = 0$. Under these conditions, Equation 4.1 simplifies to the following ordinary differential equation

$$\frac{d\hat{Y}}{dv} = -\frac{r(v) + g'(v)}{g(v)}\hat{Y} \tag{4.3}$$

where $g'(v)$ is the derivative of $g(v)$ with respect to v. Further, we introduce a combined function $f(v)$ which is a combined function of both the cyst growth $g(v)$

Table 4.1: Functions and their definitions.

Function	Biological Description
$B(t)$	The rate at which uninfected target cells are becoming infected at time t, leading to the formation of new cysts with volume v_0.
$\hat{B}$	The rate at which uninfected target cells are becoming infected at steady state.
$g(v)$	Cyst volume growth rate. Equal to the rate at which bradyzoite population is increasing within a cyst.
$g'(v)$	First derivative of the cyst growth function $g(v)$ with respect to v.
$r(v)$	Cyst removal via both immune response clearance and cyst bursting.
v_0	Volume of newly formed cysts.
$v_{\max}$	Maximum possible cyst volume.
$Y(t, v)$	Absolute density of host cells infected with cysts of volume v at time t.
$\hat{Y}(v)$	Absolute density of host cells infected with cysts of volume v at steady state.
$\hat{Y}_T$	Total density of infected host cells and equal to $\int_{v_0}^{v_{\max}} \hat{Y}(v)dv$.
$y(v)$	Relative density of host cells infected with cysts of volume v at steady state and equal to $\hat{Y}v/\hat{V}_T$

and removal $r(v)$ functions. Using the combined function, the above has a general solution of

$$\hat{Y}(v) = \hat{Y}_0 \exp\left[-\int_{v_0}^{v} f(v')dv'\right] \tag{4.4}$$

where $\hat{Y}_0$ represents the steady state density of newly formed cysts and satisfies the boundary condition defined in equation 4.2 with $B(t) = \hat{B}$. More specifically,

$$f(v) = \frac{r(v) + g'(v)}{g(v)}. \tag{4.5}$$

Because the combined function $f(v)$ is a function of both $g(v)$ and $r(v)$ the first parameters of growth and removal functions, g_0 and r_0 respectively, cannot be uniquely identified. Instead, they can be estimated only as ratios of one another, i.e. r_0/g_0.

Table 4.2: Definitions of cyst growth $g(v)$,removal $r(v)$ functions,the corresponding combined function $f(v)$, the results AIC, ΔAIC, and parameter estimates for the model selection study.

Index	Growth $g(v)$	Removal $r(v)$	Combined $f(v)$	AIC	ΔAIC	$\frac{r_0}{g_0}$	r_1
1	g_0	r_0	$\frac{r_0}{g_0}$	1915.88	0.33	0.03	N/A
2	g_0	$r_0 v$	$\frac{r_0}{g_0} v$	1990.32	74.77	0.0004	N/A
3	g_0	$r_0 v^2$	$\frac{r_0}{g_0} v^2$	2064.06	148.51	10^{-6}	N/A
4	g_0	$r_0 \frac{v}{1+v}$	$\frac{r_0}{g_0} \frac{v}{1+v}$	1916.21	0.66	0.03	N/A
5	g_0	$r_0 \frac{v^2}{1+v^2}$	$\frac{r_0}{g_0} \frac{v^2}{1+v^2}$	1915.55	0.0	0.03	N/A
6	g_0	$r_0 (1 + r_1 v)$	$\frac{r_0}{g_0} (1 + r_1 v)$	1917.88	2.33	0.03	0.0
7	g_0	$r_0 \frac{v}{r_1+v}$	$\frac{r_0}{g_0} \frac{v}{r_1+v}$	1917.87	2.32	0.03	0.07
8	g_0	$r_0 \frac{v^2}{r_1+v^2}$	$\frac{r_0}{g_0} \frac{v^2}{r_1+v^2}$	2917.12	1.57	0.03	8.74
9	$g_0 v(1 - \frac{v}{v_{\max}})$	r_0	$\frac{\frac{r_0}{g_0} v_{\max} + v_{\max} - 2v}{v_{\max} v - v^2}$	2211.24	295.69	0.24	N/A
10	$g_0 v(1 - \frac{v}{v_{\max}})$	$r_0 \frac{v}{1+v}$	$\frac{\frac{r_0}{g_0} v v_{\max} + (v_{\max} - 2v)(1+v)}{v(1+v)(v_{\max} - v)}$	2182.26	266.71	0.27	N/A
11	$g_0 v$	r_0	$\frac{1}{v} \left(\frac{r_0}{g_0} + 1 \right)$	2269.66	354.11	0.25	N/A
12	$g_0 v$	$r_0 \frac{v}{1+v}$	$\frac{1}{v} + \frac{r_0}{g_0} \left(\frac{1}{1+v} \right)$	2238.08	322.53	0.27	N/A
13	$g_0 v$	$r_0 \frac{v^2}{1+v^2}$	$\frac{1}{v} + \frac{r_0}{g_0} \frac{v}{1+v^2}$	2248.9	333.25	0.27	N/A

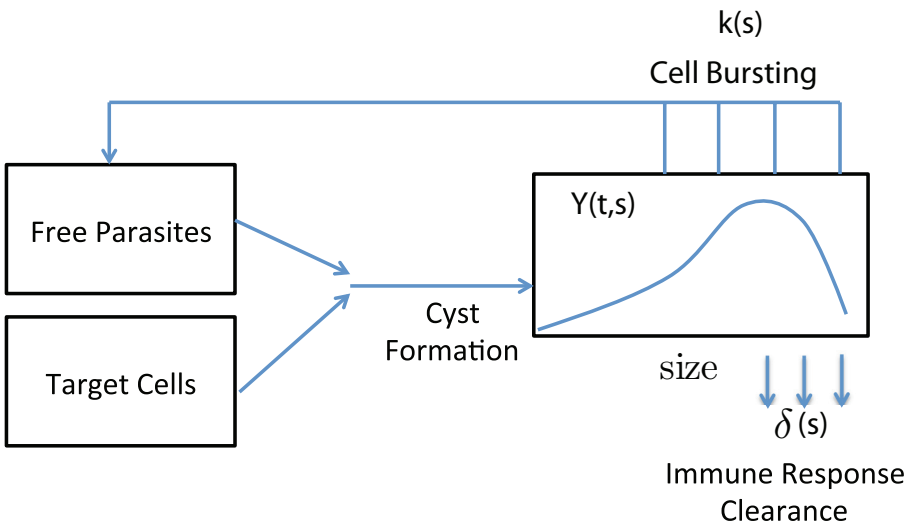

Figure 4.3: Chronic infection diagram of cyst-volume distribution model. Parasites infect healthy cells and begin replicating, causing the volume of the cyst to increase. The parasites burst at some rate and release new parasites into the system which are capable of infecting new healthy cells.

4.1.4 Fitting Models to the Cyst Volume Estimates

Our data on cyst volume represents a random sample from the larger cyst population, in order to fit our models to this data we generate a probability density function $y(v)$ from our steady state solution. We investigate the steady state solution in 4.4 under several different forms of growth and removal functions; see definitions in Table 4.2. We divide cyst density by the total cyst population size, $\hat{Y}_T = \int_{v_0}^{v_{max}} \hat{Y}(v)dv$ to get

$$y\left(v\left|\vec{\lambda}\right.\right) = \frac{\hat{Y}\left(v\left|\vec{\lambda}\right.\right)}{\hat{Y}_T\left(\vec{\lambda}\right)} = \frac{\exp\left[f\left(v\left|\vec{\lambda}\right.\right)\right]}{\int_{v_0}^{v_{\max}} \exp\left[f\left(v\left|\vec{\lambda}\right.\right)\right]}, \tag{4.6}$$

where $\vec{\lambda}$ represents the parameters of a given combined function f (e.g. r_0/g_0 or r_0/g_0 and r_1). It follows that the negative log-likelihood $\mathcal{L}$ of a particular

model and parameter set $\vec{\lambda}$ given a random sample of n observed cyst volumes $\vec{V} = \{V_1, V_2, \ldots V_n\}$ is simply,

$$\mathcal{L}(V|\vec{\lambda}) = -\sum_{i=0}^{n} \ln\left(\hat{y}\left(V_i \middle| \vec{\lambda}\right)\right) = -\left(\sum_{i=1}^{n} \ln(\hat{Y}(V_i))\right) + n \ln\left(\int_{v_0}^{v_{\max}} \hat{Y}(v)dv\right) \quad (4.7)$$

For each model in Table 4.2 we estimated the corresponding model parameters $\vec{\lambda}$ by minimizing $\mathcal{L}$ based on the observed data $\vec{V}$ using the NMinimize routine in Mathematica 8.1. The minimal $\mathcal{L}$ value and the total number of independent parameters were used to calculate the AIC value for each model. All of the results are also presented in Table 4.2.

4.2 Results

Limited amounts of data are available in the literature to quantify the steady-state volume distribution of *T. gondii* cysts [99, 72]. Qualitative evidence presented suggests that the over time distribution of cyst-volumes increases until it reaches a steady state [99]. Data from Hooshyar [72] provided a brief snapshot of the cyst distributions over time within a host. To produce more data, we conducted experiments to measure cyst volumes from 4 mice after 6 months of infection. From the 4 mice, there were 213 cyst observations that we combined into a single data set.

Three different growth functions were examined: linear, logistic, and exponential. In preliminary studies of the models presented in Table 4.2, the exponential and linear growth rate functions are clearly not supported by the data. Instead, the data clearly supported the linear growth function and thus various growth models using additional removal functions as shown in Table 4.2 were examined.

Two separate studies support our assumption that the steady state is reached by month 4. In once such study, the chronic infection of *T. gondii* reaches steady-state after 2 months while another study found the number of cysts per brain (and the copies of parasite DNA) peaked near 40-60 days [110]. The measurements we

collected were in the form of two radii of a cross-sectional area of each cyst, and thus we assumed the volume was ellipsoidal in shape, and were able to calculate the volume of the cysts. In examining the data from Hooshyar [72], we were able to make conclusions on when the dynamics of chronic infection reached stationarity. The mean volume of month 2 was 54.15 μm^3, the mean volume of month 3 was 139.15 μm^3, and the mean volume of month 4 was 107.97 μm^3. The results of comparing these three different distributions suggest there is a significant difference in mean cyst volume between month 2 and 3 (t=-1.963, $p < 0.05$), 2 and 4 (t=-2.922,$p < 0.05$), but not 3 and 4 (t=0.0685, $p < 0.05$). These results indicate that the system reaches steady-state before month 3. Therefore, our experimental design collected cyst volumes from 4 mice infected after 6 months to insure stationarity.

The Akaike Information Criteria (AIC) score was used to evaluate and compare different models [79]; see Table 4.2. The AIC value of a model is based on its negative log-likelihood at the MLE parameters and the number of parameters. The ΔAIC of a model is the difference between the lowest observed AIC value and the AIC value for a given model [27].

For comparison, probability distributions of one parameter models are shown in Figure 3.2. Typically, the distribution of cysts of *T. gondii* are viewed in terms of diameter. However, biologically volume is a more appropriate measure since it is expected to be proportional to the number of bradyzoites in a cyst. While the probability distribution on the diameter scale (Figures 6.5 (c) and (d)) is unimodal, the probability distribution on the volume scale (Figures 6.5 (a) and (b)) does not show modality. This difference is due to nonlinear transform between volume and diameter [38]. The volume of a cyst is calculated using the measured diameters plotted in Figure 4.2. The diameter scale is the geometric mean of the measurements of each cysts diameter.

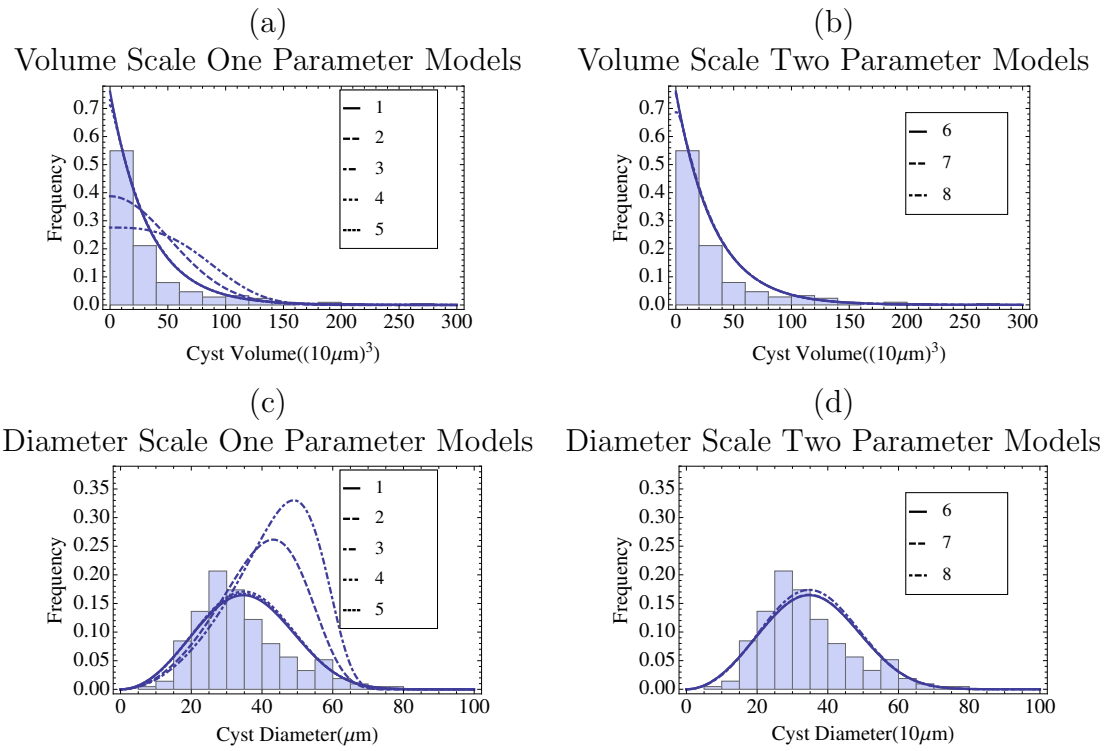

Figure 4.4: Probability distributions for one-parameter models (left) and two-parameter models (right), with the volume representation on the top and diameter scale on the bottom (the same models are presented, but represented with different transformations). For (a) and (c), the solid line represents the function $\frac{r_0}{g_0}$, the dashed line represents $\frac{\frac{r_0}{g_0}v}{1+v}$, and the dot-dashed line represents $\frac{\frac{r_0}{g_0}v^2}{1+v^2}$. For (b) and (d), the solid line represents the function $\frac{r_0}{g_0} + d_1 v$, the dashed line represents $\frac{\frac{r_0}{g_0}v}{d_1+v}$, and the dot-dashed line represents $\frac{\frac{r_0}{g_0}v^2}{d_1+v^2}$. Since two diameters were recorded, the diameter used in the data histogram is an effective diameter calculated by using $\sqrt{\frac{r_1}{2}\frac{r_2}{2}}$.

4.3 Discussion and Conclusion

We have developed a mathematical framework to select the most appropriate mathematical descriptions for the growth and removal processes through parameter fitting of experimental data. The use of various forms for the growth and removal functions demonstrate the flexibility of the model to adapt and validate on other data sets. Since the goal is to understand the behavior of cysts at the chronic stage of infection, we have used the stationary assumption of the model to match data

from chronic measurements. The parameter fitting of the steady-state solution yields multiple cases associated with each removal function. First, we considered three different growth functions along with various removal functions. It was clear that the only growth rate function that fit was the constant growth rate function. For the constant growth rate, the AIC values of the best cases for constant growth all had ΔAIC values of less than 2 (constant, type II, type III, and type III with two parameters). Based on the AIC criteria, performances of several functions (constant, type II, type III, and type III with two parameters) are indistinguishable for the constant growth rate model. Thus, the current study supports several models as the best growth and removal functions.

The most critical finding of this model selection problem is the lack of support for the linear and logistic growth rates. Normally, population growth satisfies a logistic or exponential growth function. However, experimental data here supports a constant growth rate model. The cyst volume growth is described by the following equation:

$$\frac{dv}{dt} = g(v) \tag{4.8}$$

Assume the cyst volume is proportional to the number of bradyzoites within the cyst and denote the bradyzoite number by n. Therefore, a constant volume growth rate indicates that the number of parasites within the cyst increases linearly over time and the per capita growth of bradyzoites if inversely proportional to the number of parasites. This probably suggests that bradyzoites do not replicate synchronously but instead collectively produce a single new bradyzoite at some time interval. For example, a cyst may start with a given number of bradyzoites and a single new bradyzoite may be formed through replication every few hours. While it may be surprising that the bradyzoites replicate in a way analogous to a factory producing a product, there may be factors such as nutrient availability, resource allocation, immune response, and other stress factors that may suppress synchronous replication

in cysts. Therefore, the data-driven model selection results here provide evidence for asynchronous bradyzoite division.

Understanding of the chronic infection period for *Toxoplasma gondii* will aid in understanding the role of cyst growth, bursting, and removal in the maintenance of a chronic infection. Understanding how cysts behave during chronic infection is a first step in developing a complete framework of the complete life-cycle process. Ideally, knowing the removal and growth rates from independent experiments could determine which growth and bursting functions cysts follow. However, following individual cohorts *in vivo* may not be possible experimentally and thus additional modeling experiments can be formed as a byproduct of this work.

With the development of high throughput technology [8], experiments can be designed to automatically count the number of cysts and to measurement their volumes. These data can help researchers answer important questions regarding the dynamics of cyst formation and chronic infection. Moreover, data should be collected at multiple time points, including the acute infection phase, in order to further determine transient dynamics of cyst growth and removal.

The chronic stage of *T. gondii* infection involves many complex biologic processes. The current model lumps these processes into a growth and a removal functions. Thus, the results and analyses here provide limited insights on biological details such as regulations of immune response and stage-conversion phenomena. In future work, a more detailed model will be developed to include the bursting of free parasites, invasion of free parasites into host cells, replication of tachyzoites and bradyzoites during early infection of host cells, and the cyst-volume growth functions as described here. We envision integrated experimental and analytical analyses may ultimately develop better immunological treatment plans for immunocompromised patients infected with chronic *Toxoplasma gondii*.

Chapter 5

Within-Host Dynamics ODE Model

5.1 Introduction

T. gondii has a complex life cycle, as seen in Figure 6.1. The parasite uses the feline to reproduce sexually. When the cat becomes infected, it sheds oocysts, which infect the environment. These oocysts can be ingested by mammals and birds which then become infected with the parasite [48]. Eating another organism that is infected can also infect the secondary hosts. A few mathematical models have been developed to investigate the transmission dynamics of *T. gondii* between different hosts [2, 63, 78].

Within a host, *T. gondii* exists in two interconvertable stages: bradyzoites and tachyzoites. Bradyzoites have the slow-growing and encysted form whereas tachyzoites are the fast-replicating parasites. Tachyzoites disseminate within the host and lead to the acute phase of infection. After the bradyzoite-containing cysts are ingested by the host, the walls of these cysts are digested inside the host's stomach. Bradyzoites, which are resistant to gastric conditions in the stomach, will subsequently invade the host's epithelial cells of the small intestine and convert into tachyzoites there. While most of tachyzoites in immunocompetent hosts are

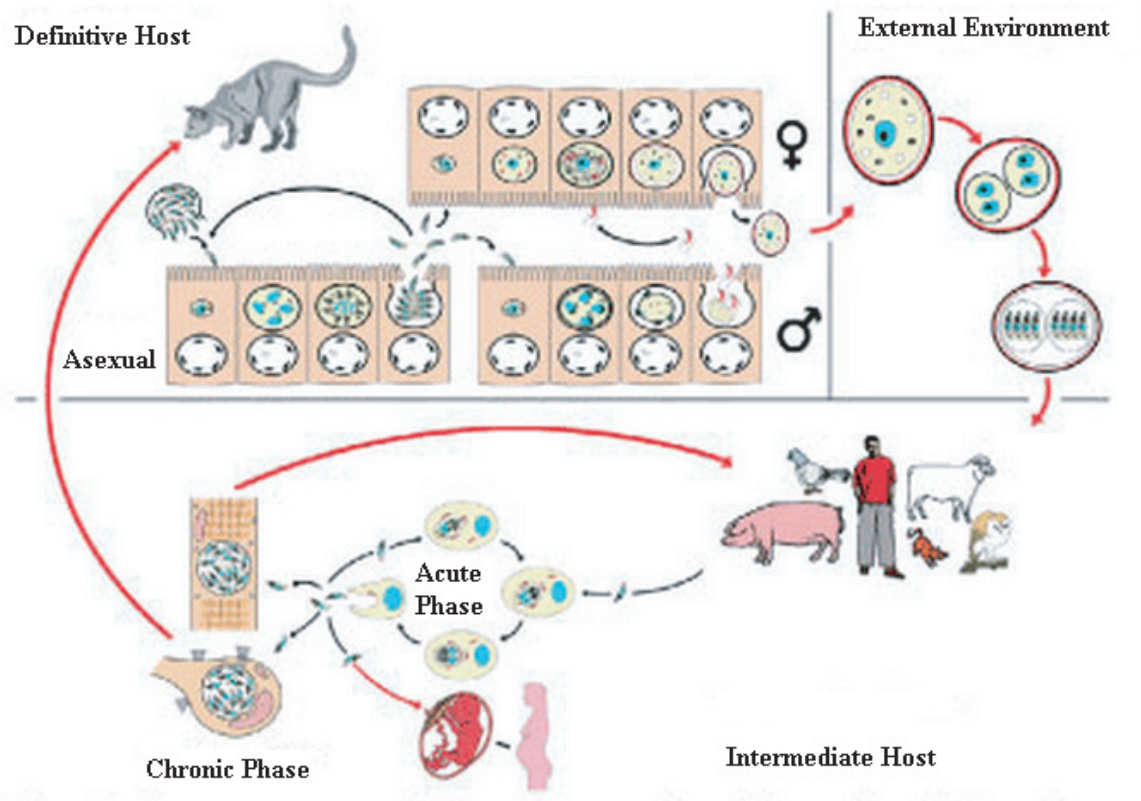

Figure 5.1: Diagram representing the life cycle of *T. gondii*. Reprinted from [45].

eliminated by the innate and adaptive immune responses, some tachyzoites differentiate into the dormant bradyzoite stage inside host cells [48]. The differentiation of tachyzoites into the bradyzoite stage plays an essential role in the development of tissue cysts, which allows life-long persistence of the parasites in the host. Reactivation of bradyzoites back to tachyzoites can lead to life threatening infection. The interconversion between tachyzoites and bradyzoites can be influenced by many in vivo and in vitro factors. In this work, we aim to develop a mathematical model to understand the nonlinear, complex interactions between *T. gondii* invasion dynamics and host immune response.

In the following sections, the results, numeral solutions, and model development were done in collaboration with those found in [123]. However, the proofs were formalized by the mathematicians of the collaboration, and I include them as supplementation to the work I have done on the project.

5.2 Model and Method

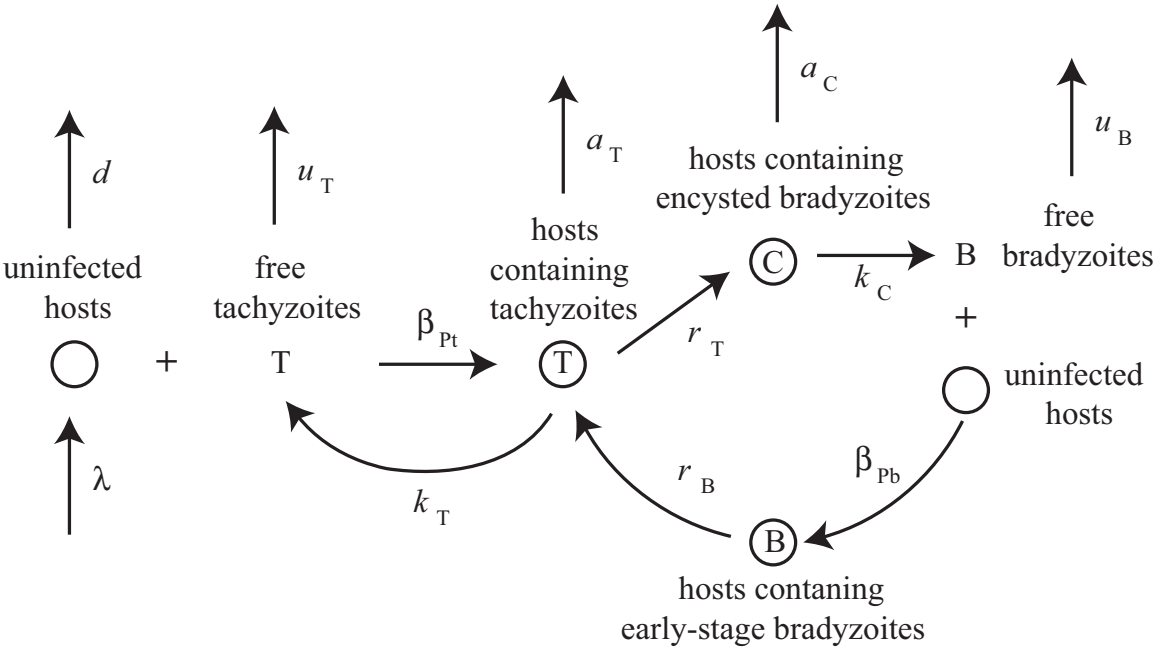

Figure 5.2: Compartmental model representing within-host invasion dynamics of *T. gondii*. Note the immune response is not shown.

We develop a compartmental model to describe the invasion dynamics of *T. gondii*; see Figure 5.2. The model has 7 state variables: the population size of uninfected cells, X; the population of cells infected with tachyzoites, Y_T; the population of cells containing early-stage bradyzoites, Y_B; the population of cells containing encysted bradyzoites, Y_C; the population of free tachyzoites, P_T; the population of free bradyzoites, P_B; and the effector cells of the host's immune response, Z.

We assume uninfected cells are generated at a constant rate of λ and assume the average life time of an uninfected cell is $1/d$. In the absence of an infection, the population dynamics of host cells is given by $\dot{X} = \lambda - dX$. Under this simple population dynamics model, the number of uninfected cells converges to the equilibrium $X_0 = \lambda/d$. Free parasites infect uninfected cells at a rate proportional to the product of their abundance: $\beta_{PT} X P_T$ for tachyzoites and $\beta_{PB} X P_B$ for bradyzoites. The rate constants, β_{PT} and β_{PB} describe the efficacy of the invasion

process and depend on the rate at which the parasites find uninfected cells, the rate of parasite entry, and the probability of successful infection. Note that β_{PT} and β_{PB} are lumped parameters and have the unit 1/(number of cells)/time [87, 105, 106, 137]. Note these rate constants sometimes carry a slightly different definition; see [24] for example.

Average life time of a cell infected with tachyzoites is $1/a_T$ and that of a cell infected with encysted bradyzoites is $1/a_C$. Since tachyzoites replicate much faster than bradyzoites, one expect a_C be much smaller than a_T. Assume the total number of parasites produced from one infected cell containing tachyzoites, i.e. the burst size, is s_T and assume the burst size of an encysted cell is s_C. Let $k_T = s_T * a_T$ and $k_C = s_C * a_C$. Then, free parasites are produce at a rate $k_T y_T$ for tachyzoites and $k_C y_C$ for encysted bradyzoites. Free parasites are removed from the system at a rate $u_T P_T$ for tachyzoites and at rate $u_B P_B$ for bradyzoites. Tachyzoites in a host cell can spontaneously convert to bradyzoites at a rate $r_T y_T$. To account for the reactivation process, we assume early-stage bradyzoites may convert to tachyzoites at a rate $r_B y_B$. We also consider a simple model for the immune response. Much work has been done regarding the immune response caused by Toxoplasma infection and many important mechanisms have been identified [56]. Here, we introduce a variable Z to represent the overall effector cells without consideration of specific immune mechanisms. We assume the effector cells act on host cells infected with tachyzoites in a predator-prey manner.

Combining the above processes leads to the following system of equations:

$$\dot{X} = d(X_0 - X) - \beta_{PT} X P_T - \beta_{PB} X P_B \tag{5.1}$$

$$\dot{Y}_T = \beta_{PT} X P_T - a_T Y_T - r_T Y_T + r_B Y_B - c_T Y_T Z \tag{5.2}$$

$$\dot{Y}_C = r_T Y_T - a_C Y_C \tag{5.3}$$

$$\dot{Y}_B = \beta_{PB} X P_B - r_B Y_B \tag{5.4}$$

$$\dot{P}_T = k_T Y_T - u_T P_T \tag{5.5}$$

$$\dot{P}_B = k_C Y_C - u_B P_B \tag{5.6}$$

$$\dot{Z} = \frac{\rho Y_T Z}{h + Y_T} - \delta Z \tag{5.7}$$

where ρ is the production rate of the effector cells, δ is the removal rate of the immune system response, and h represents the saturation level of the effector cells [137]. The first term in the immune equation represents the activation process in response to the detection of infected cells whereas the second term in the immune equation represents natural decay of the immune effector. The activation process takes the form of Holling's Type II predator-prey relation [96, 120, 30]. When the number of infected cells is small, the level of immune response is low. Then, the immune response increases at a great rate and saturates when the number of parasites is sufficiently large.

Kafsack *et al.* [83] developed a mathematical model to interpret kinetics data collected for *T. gondii* invasion. Their results show that *T. gondii* invasion dynamics including contact, attaching, penetrating, and invasion occur within a few minutes. On the other hand, previous experiments show that replication and stage conversion dynamics take place in hours [76, 48, 135]. We assume that the kinetics of free parasites are significantly faster than kinetics of other processes. Thus, we can adopt the common quasistationary approximation and assume the free parasites are

in equilibrium. It follows from Equations (5.5)-(5.6) that

$$P_T = \frac{k_T Y_T}{u_T} \tag{5.8}$$

$$P_B = \frac{k_C Y_C}{u_B} \tag{5.9}$$

Substituting the above equations into Equations (5.1)-(5.4), (5.7) leads to the following reduced model:

$$\dot{X} = d(X_0 - X) - \beta_T Y_T X - \beta_B Y_C X \tag{5.10}$$

$$\dot{Y_T} = \beta_T Y_T X - a_T Y_T - r_T Y_T + r_B Y_B - c_T Y_T Z \tag{5.11}$$

$$\dot{Y_C} = r_T Y_T - a_C Y_C \tag{5.12}$$

$$\dot{Y_B} = \beta_B Y_C X - r_B Y_B \tag{5.13}$$

$$\dot{Z} = \frac{\rho Y_T Z}{h + Y_T} - \delta Z, \tag{5.14}$$

where $\beta_T = k_T \beta_{PT}/u_T$ and $\beta_B = k_C \beta_{PB}/u_B$. A compartmental model of this simplified model is shown in Figure 5.3. All parameters in the model are non-negative and one can show that the solutions of the system are non-negative, given non-negative initial values. The model (5.10)-(5.14) will be analyzed in a biologically-feasible region as follows. We consider the region

$$\mathcal{D} = \left\{ (X, Y_T, Y_C, Y_B, Z) \in I\!R^5_+ : X \geq 0, Y_T \geq 0, Y_C \geq 0, Y_B \geq 0, Z \geq 0 \right\}.$$

Solutions of (5.10)-(5.14) starting in $\mathcal{D}$ can be shown to remain in $\mathcal{D}$ for all $t \geq 0$. Thus $\mathcal{D}$ is positively invariant and it is sufficient to consider solutions in $\mathcal{D}$. We state and prove Theorem 5.1 for non-negativity of solutions of (5.10)-(5.14) in $\mathcal{D}$.

Theorem 5.1. *Let the initial data be* $X(0) \geq 0,\ Y_T(0) \geq 0, Y_C(0) \geq 0, Y_B(0) \geq 0,$ *and* $Z(0) \geq 0$. *Then, solutions* $X(t),\ Y_T(t),\ Y_C(t),\ Y_B(t)$ *and* $Z(t)$ *of the model*

system (5.10)-(5.14) are non-negative for all $t \geq 0$. Moreover, for the model system (5.10)-(5.14), the region $\mathcal{D}$ is positively invariant.

Proof. Assume that the solution of (10)-(14) has been extended to maximal domain $[0, T^*)$; we will show the non-negativity of solutions and that there is no blow-up, giving $T^* = \infty$.

Since $X_0 > 0$ and the other terms in the right hand side (RHS) of equation (10) has X as a common factor, we have that $X(t) \geq 0$ for $t \geq 0$. Similarly, the structure of the RHS of (14) implies that $Z(t) \geq 0$ for $t \geq 0$.

Note that the structure of (11)-(13) implies that if $Y_T(0) = Y_C(0) = Y_B(0) = 0$, then $Y_T(t) = Y_C(t) = Y_B(t) = 0$ for all $0 \leq t \leq T^*$ by uniqueness of the initial boundary value problem (solution is $(X(t), 0, 0, 0, Z_0 e^{-\delta t})$ where $X' = d(X_0 - X)$).

If one of $Y_T(0), Y_C(0)$ or $Y_B(0)$ is positive, then we can show that all three components are positive on $[0, T^*)$. For example if $Y_C(t) > 0$ on $[0, \epsilon]$, by integrating the DEs for Y_B and Y_T, we obtain their positivity on $[0, \epsilon]$. On the other hand, if one of these three functions hits 0, say Y_T, let t_1 be the first time that Y_T is 0 and all three functions are positive on $(0, t_1)$. The structure of (11) with $K(t) = \beta_T X(t) - a_T - r_T - c_T Z(t)$ gives

$$Y_T(t_1) e^{\int_0^{t_1} K(s)ds} - Y_T(0) = \int_0^{t_1} e^{\int_0^t K(s)ds} r_B Y_B(t) dt,$$

which is a contradiction as the RHS is positive, $Y_T(t_1) = 0$ and $Y_T(0) \geq 0$. Continuing we conclude that D is invariant.

The structure of (10) and (14) shows that X and Z do not blow up. Note that

$$M(t) = X(t) + Y_T(t) + Y_C(t) + Y_B(t)$$

satisfies

$$M'(t) \leq d(X_0 - X(t)),$$

which means that M does not blow up. Thus we conclude $T^* = \infty$.

□

Note that for $\rho \leq \delta$, the solution to our systems (10)-(14) is bounded for all $t > 0$, but later we can prove the boundedness without that assumption.

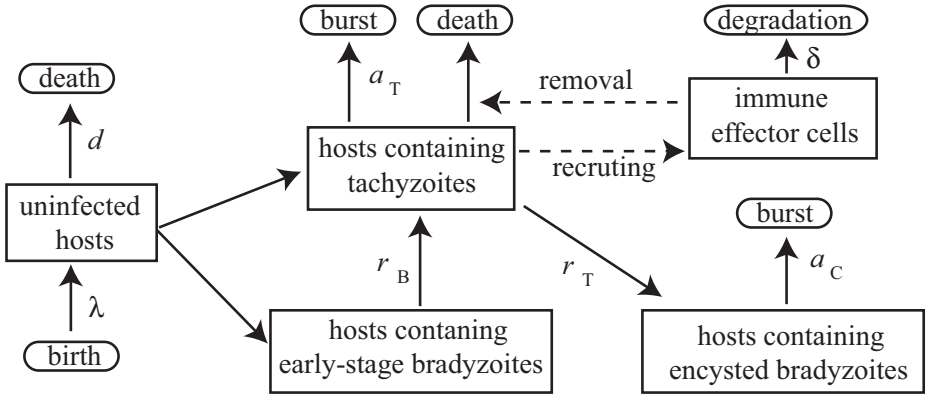

Figure 5.3: A simplified compartmental model representing the dynamics of *T. gondii*. Note the immune response is not shown.

5.3 Results

5.3.1 Disease-Free Equilibrium (DFE)

The structure of system (5.10)-(5.14) implies there exists a unique non-negative DFE solution. Denote this equilibrium solution by

$$\mathcal{E}_0 \quad = \quad (X^*, Y_T^*, Y_C^*, Y_B^*, Z^*) = (X_0, 0, 0, 0, 0). \tag{5.15}$$

The stability of $\mathcal{E}_0$ can be established using the next generation operator method on the system (5.10)-(5.14). We take, Y_T, Y_C, Y_B, as our infected compartments, then using the notation in [133], the Jacobian matrices F and V for the new infection terms and the remaining transfer terms are respectively given by,

$$F = \begin{pmatrix} \beta_T X^* & 0 & 0 \\ 0 & 0 & 0 \\ 0 & \beta_B X^* & 0 \end{pmatrix} \text{ and } V = \begin{pmatrix} a_T + r_T & 0 & -r_B \\ -r_T & a_C & 0 \\ 0 & 0 & r_B \end{pmatrix}. \tag{5.16}$$

It follows that the basic reproduction number of the system (5.10)-(5.14), denoted by $\mathcal{R}_0$, is given by

$$\mathcal{R}_0 = \rho(FV^{-1}) = \frac{X_0(a_C\beta_T + r_T\beta_B)}{a_C(a_T + r_T)} \tag{5.17}$$

where ρ is the spectral radius. Further, using Theorem 2 in [133], the following result is established.

Lemma 5.1.1. *The DFE of the model (5.10)-(5.14), given by $\mathcal{E}_0$, is locally asymptotically stable (LAS) if $\mathcal{R}_0 < 1$, and unstable if $\mathcal{R}_0 > 1$.*

The basic reproduction number ($\mathcal{R}_0$) measures the average number of new infections generated by a single infected individual in a completely susceptible population [9, 44, 68, 133]. Thus, Lemma 5.1.1 implies that *T. gondii* can be eliminated from within the host (when $\mathcal{R}_0 < 1$) if the initial sizes of the sub-populations are in the basin of attraction of the DFE, $\mathcal{E}_0$.

Consider the domain

$$\mathcal{D}_1 = \{(X, Y_T, Y_C, Y_B, Z) \in \mathcal{D} : X^* \geq X\}.$$

Using the approach in the proof of Theorem 5.1, it can be shown that the region is positively-invariant.

Theorem 5.2. *The DFE of the model (5.10)-(5.14), given by $\mathcal{E}_0$, is global asymptotically stability (GAS) in $\mathcal{D}_1$ whenever $\mathcal{R}_0 < 1$.*

Proof. The proof is based on using a comparison theorem. The equations for the infected components in (5.10)-(5.14) can be written in terms of

$$\begin{pmatrix} \frac{dY_T(t)}{dt} \\ \\ \frac{dY_C(t)}{dt} \\ \\ \frac{dY_B(t)}{dt} \end{pmatrix} = \Big(F - V\Big) \begin{pmatrix} Y_T(t) \\ \\ Y_C(t) \\ \\ Y_B(t) \end{pmatrix} - MQ \begin{pmatrix} Y_T(t) \\ \\ Y_C(t) \\ \\ Y_B(t) \end{pmatrix}, \tag{5.18}$$

where, $M = X^* - X\,(t)$, the matrices F and V are given above and Q is the non-negative matrix given by

$$Q = \begin{pmatrix} \beta_T & 0 & 0 \\ 0 & 0 & 0 \\ 0 & \beta_B & 0 \end{pmatrix}$$

Since $M \geq 0$ for all $t \geq 0$, it follows that

$$\begin{pmatrix} \frac{dY_T(t)}{dt} \\ \\ \frac{dY_C(t)}{dt} \\ \\ \frac{dY_B(t)}{dt} \end{pmatrix} \leq \Big(F - V\Big) \begin{pmatrix} Y_T(t) \\ \\ Y_C(t) \\ \\ Y_B(t) \end{pmatrix}. \tag{5.19}$$

Using the fact that the eigenvalues of the matrix $F-V$ all have negative real parts (see the local stability result given in Lemma 5.1.1, where $\rho(FV^{-1}) < 1$ if $\mathcal{R}_0 < 1$ which is equivalent to $F - V$ having eigenvalues with negative real parts when $\mathcal{R}_0 < 1$ [133]), it follows that the differential inequality system (5.19) is stable whenever $\mathcal{R}_0 < 1$. Consequently, $(Y_T(t), Y_C(t), Y_B(t)) \to (0, 0, 0)$ as $t \to \infty$. by standard comparison results [90, 53].

The structure of the X DE gives the convergence of $X(t) \to X^*$ as $t \to \infty$. Using the convergence of $Y_T(t)$ to 0 and the term with Y_T in (14) will be smaller than the δZ term for large t, we obtain that $Z(t) \to 0$.

Thus, $(X(t), Y_T(t), Y_C(t), Y_B) \to (X^*, 0, 0, 0, 0)$ as $t \to \infty$ for $\mathcal{R}_0 < 1$. Hence, the DFE $\mathcal{E}_0$ is GAS if $\mathcal{R}_0 < 1$. □

Note that the boundedness of the solutions follows in this case.

The above result shows that *T. gondii* will be eliminated from within the host if the threshold quantity $\mathcal{R}_0$ can be brought to a value less than unity.

5.3.2 Endemic Equilibrium (EE)

Let $\mathcal{E}_1 = (X^*, Y_T^*, Y_C^*, Y_B^*, Z^*)$ be any arbitrary equilibrium of the model (5.10)-(5.14). Conditions for the existence of equilibria for which *T. gondii* is endemic within the host (where at least one of the infected variables is non-zero) can be obtained as follows. Let,

$$\lambda_1^* = \beta_T Y_T^* \quad \text{and} \quad \lambda_2^* = \beta_B Y_C^*,$$

and let

$$x^* = \lambda_1^* + \lambda_2^* \tag{5.20}$$

be the associated force of infection, which is defined as the rate at which susceptible individuals become infected by an infectious disease [3, 52, 59, 58, 66, 117, 116]. To determine the existence of the endemic equilibrium, we consider first the case where immunity is not present (i.e $Z = 0$). Setting the right-hand sides of the model to zero gives the following expressions (in terms of λ_1^* and λ_2^* at steady state):

$$
\begin{aligned}
X^* &= \frac{dX_0}{(d+\lambda_1^*+\lambda_2^*)} \\
Y_T^* &= \frac{dX_0(\lambda_1^*+\lambda_2^*)}{(a_T+r_T)(d+\lambda_1^*+\lambda_2^*)} \\
Y_C^* &= \frac{dX_0 r_T(\lambda_1^*+\lambda_2^*)}{a_C(a_T+r_T)(d+\lambda_1^*+\lambda_2^*)} \\
Y_B^* &= \frac{dX_0\lambda_2^*}{r_B(d+\lambda_1^*+\lambda_2^*)}.
\end{aligned} \tag{5.21}
$$

Substituting the expression in (5.21) into the expression in (5.20) we have that the non-zero equilibrium of the model after some algebraic manipulation satisfy:

$$x^* = d(\mathcal{R}_0 - 1). \tag{5.22}$$

It follows that $x^* > 0$ if and only if $\mathcal{R}_0 > 1$. This result is summarized below:

Theorem 5.3. *The model (5.10)-(5.14) with $Z = 0$ has a unique endemic equilibrium whenever $\mathcal{R}_0 > 1$.*

Next we consider the case where the immune system responds throughout infection period (i.e $Z \neq 0$). To determine the existence of the endemic equilibrium, setting the right-hand sides of the model to zero gives the following expressions:

$$
\begin{aligned}
X^{**} &= \frac{dX_0}{(d+\lambda_1^{**}+\lambda_2^{**})} \\
Y_T^{**} &= \frac{\delta h}{(\rho-\delta)} \\
Y_C^{**} &= \frac{r_T \delta h}{a_C(\rho-\delta)} \\
Y_B^{**} &= \frac{dX_0\lambda_2^{**}}{r_B(d+\lambda_1^{**}+\lambda_2^{**})} \\
Z^{**} &= \frac{d(\lambda_1^{**}+\lambda_2^{**})(\rho-\delta)X_0 - \delta h(d+\lambda_1^{**}+\lambda_2^{**})(r_T+a_T)}{\delta h C_T(d+\lambda_1^{**}+\lambda_2^{**})}.
\end{aligned} \tag{5.23}
$$

Substituting the expression in (5.23) into the expression in (5.20) gives

$$
x^{**} = \frac{\delta h(a_T+r_T)(\mathcal{R}_0-1)}{(\rho-\delta)} + \frac{\delta h(a_T+r_T)}{(\rho-\delta)} \tag{5.24}
$$

It follows that $x^{**} > 0$ if and only if $\mathcal{R}_0 > 1$ and $\rho > \delta$. This result is summarized below:

Theorem 5.4. *The model (5.10)-(5.14) with immune response (i.e., $Z(t) > 0$) has a unique endemic equilibrium whenever $\mathcal{R}_0 > 1$ and $\rho > \delta$.*

Thus, to obtain a unique endemic equilibrium, Theorem 5.4 implies that in the presence of immune response, ρ, the maximum attack rate, must be greater than δ, the removal rate of the immune system response for this case to happen.

5.3.3 Local stability of the endemic equilibrium (EE)

In this Section we will consider the stability of the endemic equilibrium $\mathcal{E}_1$. First we consider the case without immune response ($Z = 0$); thus linearizing (5.10)-(5.14) we

have the matrix J evaluated at $\mathcal{E}_1$ with $Z(t) = 0$, using the equilibrium (5.21)

$$J = \begin{bmatrix} -d - \beta_T Y_T^* - \beta_B Y_C^* & -\beta_T X^* & -\beta_B X^* & 0 \\ \beta_T Y_T^* & \beta_T X^* - (a_T + r_T) & 0 & r_B \\ 0 & r_T & -a_C & 0 \\ \beta_B Y_C^* & 0 & \beta_B X^* & -r_B \end{bmatrix}.$$

The matrix J has the sign pattern $J_{11} < 0,\ J_{33} < 0,\ J_{44} < 0,\ J_{12}J_{21} < 0,\ J_{13}J_{31} = 0,\ J_{14}J_{41} = 0,\ J_{23}J_{32} = 0,\ J_{24}J_{42} = 0,\ J_{34}J_{43} = 0$, and $J_{22} = \frac{(a_T+r_T)(\beta_T a_C - 1)}{(a_C\beta_T + r_T\beta_B)} < 0$ provided $\beta_T a_C < 1$, thus the matrix is sign stable and hence the equilibrium (5.21) is locally asymptotically stable [1, 25, 75]. We have thus established the following result:

Lemma 5.4.1. *The endemic equilibrium (5.21) without immune response is locally asymptotically stable for $\beta_T a_C < 1$.*

Next we consider the stability of the equilibrium $\mathcal{E}_1$ in the presence of immune response (i.e., $Z(t) > 0$). Linearizing (5.10)-(5.14) evaluated at $\mathcal{E}_1$, using the equilibrium (5.23) gives the matrix J

$$J = \begin{bmatrix} -d - \beta_T Y_T^{**} - \beta_B Y_C^{**} & -\beta_T X^{**} & -\beta_B X^{**} & 0 & 0 \\ \beta_T Y_T^{**} & \beta_T X^{**} - (a_T + r_T + C_T Z^{**}) & 0 & r_B & C_T Y_T^{**} \\ 0 & r_T & -a_C & 0 & 0 \\ \beta_B Y_C^{**} & 0 & \beta_B X^{**} & -r_B & 0 \\ 0 & \frac{\rho Z^{**}}{(h+Y_T^{**})} - \frac{\rho Y_T^* Z^{**}}{(h+Y_T^{**})^2} & 0 & 0 & \frac{\rho Y_T^{**}}{(h+Y_T^{**})} - \delta \end{bmatrix}$$

The matrix J has the sign pattern $J_{11} < 0,\ J_{33} < 0,\ J_{44} < 0,\ J_{55} = 0,\ J_{12}J_{21} < 0,\ J_{13}J_{31} = 0,\ J_{14}J_{41} = 0,\ J_{15}J_{51} = 0,\ J_{23}J_{32} = 0,\ J_{24}J_{42} = 0,\ J_{25}J_{52} = 0,\ J_{34}J_{43} = 0,\ J_{35}J_{53} = 0,\ J_{45}J_{54} = 0,\ J_{22} = -\frac{r_T\beta_B X^{**}}{a_C} < 0$ and
$J_{25}J_{52} = \frac{(\rho-\delta)(a_C\beta_T + r_T)[dX_0(\rho-\delta) - h\delta(a_T+r_T)] - a_C^2 d(\rho-\delta)^2(a_T+r_T)}{h\delta\rho(a_C\beta_T+r_T) + \rho a_C d(\rho-\delta)} < 0$ provided $dX_0(\rho-\delta) < h\delta(a_T + r_T)$, thus the matrix is sign stable and hence the equilibrium (5.23) is locally asymptotically stable [1, 25, 75]. We have thus established the following result:

Lemma 5.4.2. *The endemic equilibrium (5.23) with immune response is locally asymptotically stable provided* $dX_0(\rho - \delta) < h\delta(a_T + r_T)$.

5.4 Discussion and Conclusion

Recall from (5.17) that the reproduction number $\mathcal{R}_0$ is proportional to X_0, the total number of host cells before invasion of the parasites. Assuming the invasion and reproduction kinetics of the parasites are the same in different organs, larger organs intend to have more cells and thus larger $\mathcal{R}_0$ values, which will make them more suitable for the parasites to dwell. This is probably why *T. gondii* is most frequently found in brain, heart, and muscle in a host [48]. To investigate the influences of various parameters to the diseased state, we will rewrite the endemic equilibria in terms of model parameters. The equilibrium without immune response in (5.21) can be rewritten in terms of model parameters as follows:

$$\begin{aligned} X^* &= \tfrac{X_0}{\mathcal{R}_0} \\ Y_T^* &= \tfrac{d\,X_0}{a_T+r_T} - \tfrac{d\,a_C}{r_T\,\beta_B+a_C\beta_T} \\ Y_C^* &= \tfrac{r_T\,Y_T^*}{a_C} \\ Y_B^* &= \tfrac{\beta_B\,X^*Y_C^*}{r_B}. \end{aligned} \tag{5.25}$$

It follows from (5.25) that, in endemic state, the number of healthy cells, X^*, is less than the original number of cells, X_0. The model predicts that the steady state of the disease reaches a dynamic balance between three different stages of the parasites: Y_T^*, Y_C^*, and Y_B^*. Note that Y_B^* and Y_C^* are proportional to Y_T^* and Y_T^* is positively correlated to X_0. Thus, steady state parasite loads are related to the size of the organ. Also, recall the reproduction rate of uninfected cells is $\lambda = d\,X_0$. Assume the

reproduction rate λ is a constant, it can be seen from (5.25) that, an organ with longer life expectance $1/d$ will have larger parasite loads. Since brain cells are permanent, this also explains why *T. gondii* is mostly like to be found in brain [48].

The equilibrium with immune response in (5.23) can be rewritten in terms of model parameters as follows:

$$\begin{aligned} X^{**} &= \frac{a_C\, d\, X_0(\rho-\delta)}{h\ \delta(a_C\,\beta_T+r_T\,\beta_B\,)+a_C d(\rho-\delta)} \\ Y_T^{**} &= \frac{h\,\delta}{\rho-\delta} \\ Y_C^{**} &= \frac{r_T\, Y_T^{**}}{a_C} \\ Y_B^{**} &= \frac{\beta_B\, X^{**}\, Y_C^{**}}{r_B} \\ Z^{**} &= \frac{X^{**}\,(r_T\,\beta_B + a_C\,\beta_T)-a_C(\,a_T+r_T)}{a_C\, c_T}. \end{aligned} \tag{5.26}$$

It is interesting to note that the relationships between the three parasite loads, Y_T^{**}, Y_C^{**}, and Y_B^{**}, remain the same as those in the absence of immune response although the steady state value of Y_T^{**} is now determined by kinetics of immune response. We also note the parasite loads Y_T^{**} and Y_C^{**} do not depend on the original number of host cells X_0 whereas the load Y_B^{**} is proportional to X_0. Moreover, when the reproduction rate of uninfected cells $\lambda = d\,X_0$ is kept at a constant, a larger life expectance $1/d$ will lead to a larger value of X^{**} and thus a higher parasite load Y_B^{**}. Again, the analysis shows that *T. gondii* favors cells with long life expectance such as the brain.

5.4.1 Numerical Simulations

In order to investigate the effects of *T. gondii* infection, we first introduce model assumptions and estimate parameters of infection dynamics using experimental data available in the literature. Numerical simulations here use a mouse spleen as an

example. We estimate a healthy spleen has $X_0 = 10^8$ cells. Assume that the life expectancy of spleen cells is 1 month, which leads to the death rate as $d = 1.389 \times 10^{-3}\text{h}^{-1}$. In the current model, we assume at most one parasitophorous vacuole (PV) can form within a host cell. We further assume parasites within the same PV are in the same stage and replicate simultaneously. Experimental data in Weiss and Kim [135] indicate that the doubling time of tachyzoites is 6 hours and that of bradyzoites is 24 hours. Tachyzoites *in vivo* often lyse the host cell after reproducing 2 or 3 times [35]; thus, we choose $a_T = 1/(18\text{h})$ and $k_T = 8/(18\text{h})$. Cysts of bradyzoite may contain more than 1000 parasites [47]. We assume encysted brayzoites burst after reproducing 10 times and thus estimate $a_C = 1/(240\text{h})$ and $k_C = 1024/(240\text{h})$. After a parasite is released from a PV into the organ, we assume the parasite may interact with 10 host cells and the probability of invasion of individual host is 2%. It follows that $\beta_T = 8.889 \times 10^{-10}(\text{number of cells})^{-1}\text{h}^{-1}$ and $\beta_B = 8.533 \times 10^{-9}(\text{number of cells})^{-1}\text{h}^{-1}$. Since tachyzoites can convert to bradyzoites after about 20 generations of reproduction [81], we estimate $r_T = 1/\left(108\text{h}\right)$. Weiss and Kim [135] showed that 48 hours after bradyzoites invade a tissue, tachyzoites start to appear; thus, we estimate $r_B = 1/\left(48\text{h}\right)$. The current model does not consider detailed immune mechanisms. Instead, we consider the effector cells of the immune system acting on tachyzoites in PV. Assume the interaction rate between effector cells and tachyzoite PVs as $c_T = 1.67 \times 10^{-8}(\text{number of cells})^{-1}\text{h}^{-1}$. Assume the degradation rate of the immune effector cells to be $\delta = 1/\left(48\text{h}\right)$. Let $h = 10^5$ to account for the memory effect of immune response and let $\rho = 10/\left(24\text{h}\right)$ be the response rate.

Substituting the above parameters into Equation (5.17) yields $R_0 = 30.63$, which indicates that an infected cell will, on average, infect 30.63 uninfected host cells per hour. Consider an immuno-incompetent host, in which $Z = 0$, it follows that the equilibrium diseased state is $X^* = 3.26 \times 10^6$, $Y_T^* = 2.07 \times 10^6$, $Y_B^* = 6.16 \times 10^6$, and $Y_C^* = 4.61 \times 10^6$. The total number of cells is 1.61×10^7, which is reduced to 16% of the original number, X_0. In contrast, in an immunocompetent host, the long term solution is $X^* = 9.30 \times 10^7, Y_T^* = 5.26 \times 10^3$, $Y_B^* = 4.46 \times 10^5, Y_C^* = 1.17 \times 10^4$ and

$Z^* = 1.07 \times 10^8$. The total number of cells is 9.34×10^7, only slightly less than the number for disease free state. Transient responses in the absence of immune response are shown in Figure 5.4 while transient responses in the presence of immune response are shown in Figure 5.5.

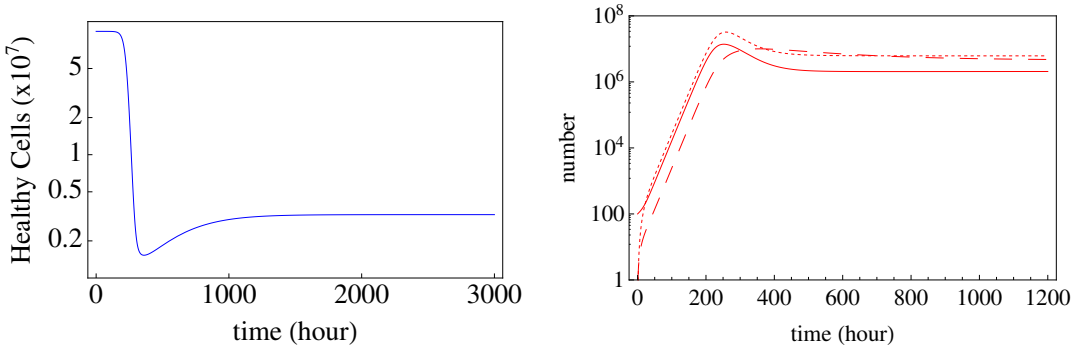

Figure 5.4: Response in the absence of immune response: variation of healthy host cells (left) and variation of infected host cells (right). The infected host cells include those infected with tachyzoites (solid), cysted bradyzoites (dashed), and early-stage bradyzoites (dotted).

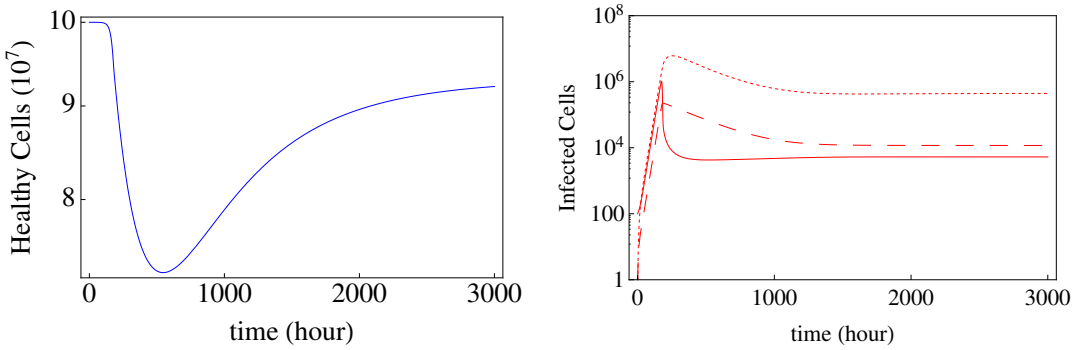

Figure 5.5: Response in the presence of immune response: variation of healthy host cells (left) and variation of infected host cells (right). The infected host cells include those infected with tachyzoites (solid), cysted bradyzoites (dashed), and early-stage bradyzoites (dotted).

We further use the model to study reactivation. While the number of parasites in an immunocompetent host is greatly suppressed, the parasites can be reactivated when the host becomes immunoincompetent [36]. Here, we consider reactivation due to temporary impairment in the immune system. We assume a host is first

infected with *T. gondii* and, after 3000 hours, the host's immune system is temporarily impaired so that the production rate ρ is reduced to 10% of the nominal value. We assume the impairment lasts for 200 hours and then the host's immunity recovers to the original level. This scenario would be analogous to a host suffering from immunodepression for a few weeks before overcoming the secondary infection and allowing for a full immune response to the toxoplasma. The results for this particular situation are shown in figure 5.6. It is clear that this temporary decrease in immune response leads to a significant increase of parasite load within the host.

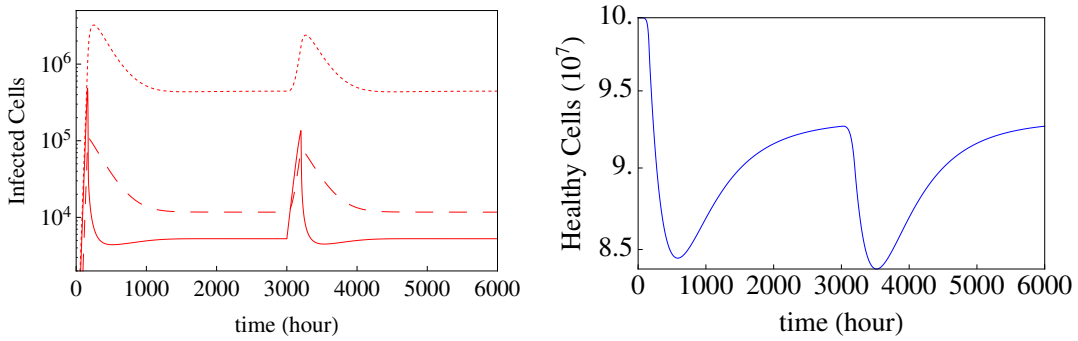

Figure 5.6: Reactivation of parasites due to temporary impairment of the immune system: variation of healthy host cells (left) and variation of infected host cells (right). The infected host cells include those infected with tachyzoites (solid), cysted bradyzoites (dashed), and early-stage bradyzoites (dotted).

Here, we have developed a mathematical framework to investigate intra-host dynamics of *T. gondii*. Assumptions and simplifications have been made about the biological processes including invasion, replication, and stage conversion. Parameters of the model have been estimated based on available experimental data. In the differential equation model we created, the effects of spreading parasites are examined. In the analysis, we first found the fixed points and analyzed the rate of infection R_0. The first fixed point in the analytical model was the parasite-free equilibrium point. The second and third equilibrium points are identical in expressions for Y_T, Y_C, and Y_B. It is interesting to note that the second and third equilibrium

points vary in the values for the immune response fixed point. The immune regulated equilibrium only exists when $\rho > \delta$.

It is also important to note the assumption made in analyzing this model. We have assumed the invasion dynamics of the free parasites are much faster than the replication and stage conversion, which leads to quasistationary simplification of the free parasites. This assumption is valid because the bursting of cells with tachyzoites release free tachyzoites, this release was modeled as a contribution of infection directly to uninfected hosts. The use of the Holling's Type II functional response models the way an immune system should respond: Very limited response to low numbers of invaders and a quickly growing response up to a threshold as the number of invaders increases. This type of response allows us to simplify the immune system into a mathematical model.

The critical value for R_0 found in this model indicates that our infection rate is dependent upon the initial number of uninfected hosts, the death rate of cells infected with bradyzoites and tachyzoites, the invasion rate of tachyzoites and bradyzoites contained within a host, and the conversion rate from tachyzoites to bradyzoites. Analyses of the reproduction number and the endemic solutions indicate that *T. gondii* favors large organs with long life expectance. This agrees with the experimental observation that *T. gondii* are commonly found in skeletal muscles, brain, and myocardium.

Numerical simulations show that the immune system plays a pivotal role in suppressing the growth of tachyzoites within host cells. This suppression, once the system reaches endemic behavior, allows for the body to exit the acute infection stage and begin the long-term, virtually symptom-free, state. Without immune response, the tachyzoites would be free to replicate and invade many different hosts.

Tachyzoites are rapidly dividing and responsible for the acute infection whereas the slowly replicating bradyzoites are located within tissue cysts, which protect the parasite from the host immune system and make it inaccessible to drugs [48]. The differentiation of tachyzoites into bradyzoites is a response to the onset of protective

immunity whereas the dormant bradyzoites are able to reconvert into tachyzoites to cause fatal infection in patients. Therefore, stage conversion between tachyzoites and bradyzoites plays a pivotal role in the pathogenesis, transmission, persistence, and reactivation of the disease.

Future work of this system will include a more detailed description of immune response. While using the Holling's Type may accurately model the conceptual framework of an immune response, more evidence is needed to qualify this technique as accurate. A further expansion of this model might include a spatial array in which the disease can propagate. While our model tracks the disease throughout the spleen and assumes a homogenous distribution of cells throughout, the parasites are actually capable of starting in the stomach and invading the brain, muscles, and liver. Therefore, a spatial model may be able to describe the complicated dynamics that describe how the parasites can move throughout the body.

Chapter 6

Cellular Automata Brain Simulation of Infection

6.1 Introduction

Toxoplasma gondii is a parasitoid that infects up to 20% of the world's population [4]. While the parasite does not typically cause death when an individual becomes infected with *Toxoplasma*, those with deficient immune systems can develop severe brain inflammation. Additionally, infection during pregnant can cause severe birth defects. The effect it has on humans makes this an important parasite to study and monitor, especially the mechanisms that regulate the within-host dynamics.

Toxoplasma gondii is a parasite that infects mammals and birds. The parasite uses the feline to reproduce sexually. When the cat becomes infected, it sheds oocysts, which infect the environment. These oocysts can be ingested by mammals and birds which then become infected with the parasites [80]. Eating another organism that is infected can also infect the secondary hosts.

The life cycle of a parasite starts out as a tachyzoite which replicates asexually very quickly. The tachyzoites infect host cells, where they feed off of the nutrients in the host to reproduce. Once the parasite replicate several times , they will burst

from the host cell and continue to search for a new host and infect other host cells. Sometimes, the host cell will not burst and the parasites will convert to a new stage of *Toxoplasma* known as a bradyzoite. These parasites replicate very slowly and will eventually turn a host cell into a cyst (most often in muscle and brain tissue). These cysts are filled with thousands of bradyzoites, and can remain alive even after a host has died. The consumption of undercooked meat is one way to release a bradyzoite cyst [4].

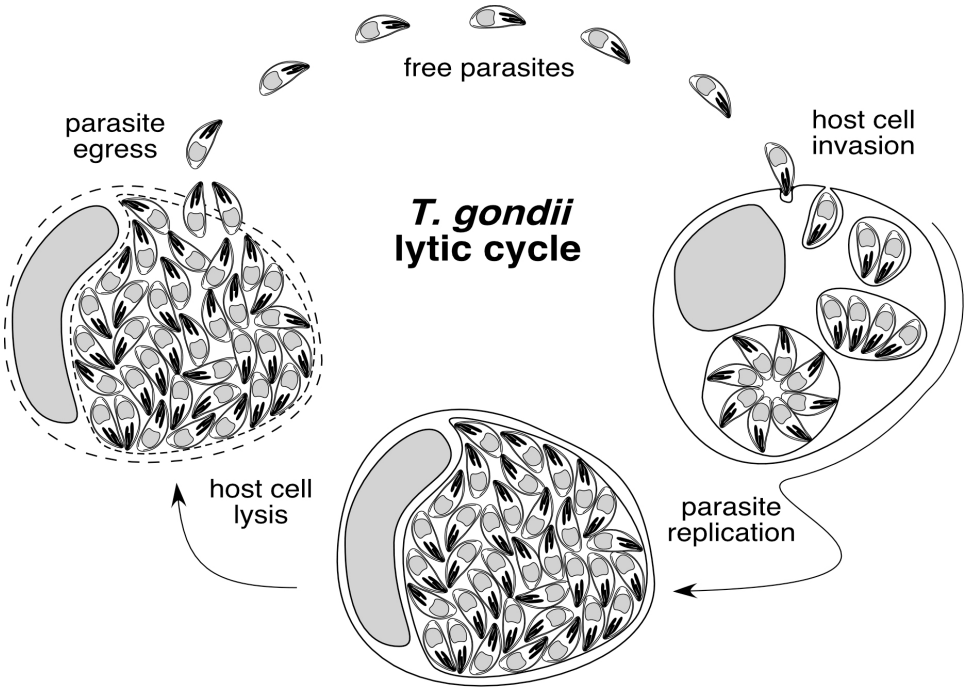

Figure 6.1: Life cycle representation of *Toxoplasma gondii* from [65]. The parasites invade a host cell, replicate within the host cell, and eventually burst, releasing new parasites capable of reinvasion of a host cell.

Once a host cell containing bradyzoites bursts, each bradyzoite can then reinvade other healthy host cells, thus completing the life cycle within the host. This work focuses solely on the asexual replication cycle of the parasite and does not consider sexual replication within a cat.

Toxoplasma gondii is unique in that parasites can exist in the tachyzoite or bradyzoite state throughout the life cycle. Tachyzoites are rapidly dividing and

responsible for the acute infection whereas the slowly replicating bradyzoites are located within tissue cysts, which protect the parasite from the host immune system and make it inaccessible to drugs [80]. The differentiation of tachyzoites into bradyzoites is a response to the onset of protective immunity whereas the dormant bradyzoites are able to reconvert into tachyzoites to cause fatal infection. We also investigate the effects of different hypothesized growth functions have on the pathogenesis, transmission, persistence, and reactivation of the disease.

6.2 Model and Method

6.2.1 Cellular Automata

A simple cellular automata model requires four components: a spatial domain, a set of states that can exist, a set of neighborhoods, and deterministic rules. To develop our model, we define our cellular automata in the following manner.

The spatial domain the geographic mesh of an organ or tissue we are studying. The spatial domain is a set of nodes identified on a tetrahedral mesh. Each node contains a given number of actual cells. Additionally, each node is capable of possessing a number of free tachyzoites or bradyzoites. These free tachyzoites or bradyzoites are capable of invading the host cells contained within each node.

We define the cells to have the states of Y_T for a cell infected with tachyzoites, Y_C for a cell infected with cysted bradyzoites, and Y_B for a cell infected with recently freed bradyzoites (these typically convert back to tachyzoites). Additionally, a cell's state is dependent upon the the number of parasites contained within it, because the rule definitions change with the number of parasites within each host cell. Therefore, it is necessary to label the state of each cell with the number of parasites of each type contained within the cell. There are two neighborhood definitions. Each cell in the sub-domain of each node has a local neighborhood of every other cell within the same sub-domain. Every node has a neighborhood calculated by finding other nodes

within a given radius. Figure 6.2 paints a picture of how a node is defined within the context of our model.

The update rules are all based on phenomenon expressed by the *T. gondii* parasite and their reaction with host cells. These rules are presented in the next section. The simulation applies all of the rules before moving on to the next time step. The default time step for the algorithm is 1 hour, although different time steps may be specified.

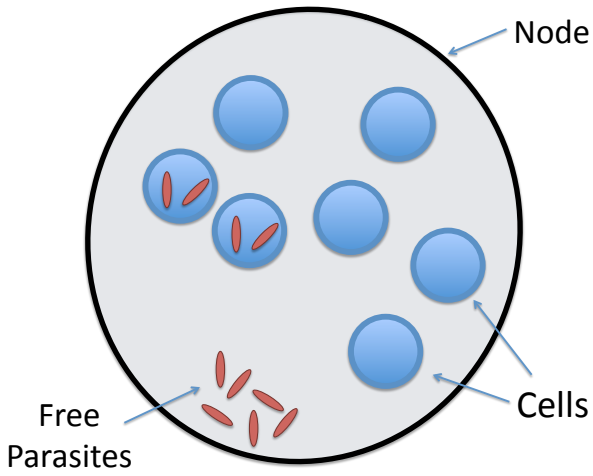

Figure 6.2: Figure of a node that includes some healthy cells, infected cells, and free parasites. The node is an object and each cell is an object within each subdomain of a node. The free parasites and invaded parasites are maintained as variables within each object.

6.2.2 Biological Rules

The *Toxoplasma gondii* parasites behaves in a way that makes it possible to model the biological processes using simple rule updates. We have modeled the various rules using functions within each object. Rules are updated within each node and within each cell. A flow diagram of the assumptions is presented in Figure 6.3.

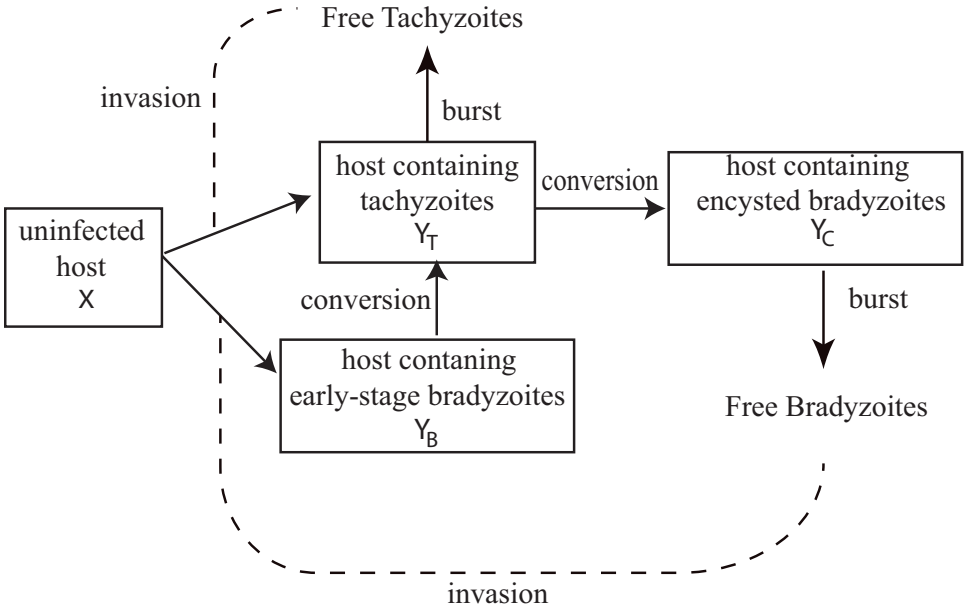

Figure 6.3: Flow diagram of the biological processes and assumptions presented in this model. This figure is modified from [123].

Invasion

A free parasite in either the tachyzoite or bradyzoite state is able to move about the organ by moving from node to node. Transitioning from one node to the next depends on whether the parasite can overcome the probability of a free parasite dying. Otherwise, the free parasite may enter any one of the pre-calculated neighboring nodes from its current node with equal probability. We define p_t, the probability of transition, to be $\frac{1}{n_i+1}$, where n_i is the number of neighboring nodes available to the ith node. The number of neighbors is found by calculating all neighboring nodes within a given radius of a node.

A free parasite follows three processes when invading a host cell contained within a node. Firstly, a parasite will invade a host cell with a given probability. Secondly, a parasite can only invade a host cell that does not contain any parasites. Thirdly, a parasite, if unsuccessful at invading the first host cell, can attempt to invade each

healthy host-cell until it has tried each cell. After it has tried to invade each cell, the process will stop.

Replication

Once a parasite invades a healthy cell, the process of replication begins. The replication rate for tachyzoites and bradyzoites is specified within the algorithm (see Table 6.1). A tachyzoite may replicate at a rate of r_T.

To investigate varying degrees of replication of bradyzoites, we consider three different growth functions:

- synchronous replication of the cyst: for a true probability event, all parasites will replicate once.
- asynchronous replication of the cyst: for a true probability event, a given number of parasites will be added to the cyst.
- individual replication of individual parasites: each parasite within a cyst will undergo a probability event, and if true, a single parasite will be added to the cyst population of bradyzoites.

A moderate immune response may contribute to bradyzoite conversion by suppressing parasite replication but still allowing parasites to reach a pre-mitotic cell cycle checkpoint for entry into conversion [121]. This type of immune response is seen in several mathematical models used in tumor modeling [85]. The bradyzoites are formed in to cysts and develop stability as they grow. A combination of immune response and self-regulation within the cyst causes the bradyzoites to slow down from their initial replication rate. This reduction in the replication rate of encysted bradyzoites is

$$p_{\text{rep}} = r_C \left(1 - \frac{C}{N_C}\right) \tag{6.1}$$

where r_C is the probability of a replication event of bradyzoites, C is the number of bradyzoites within the cyst, and N_C is the maximum observable number of parasites

possible within a cyst. This response is modeled in such a way that the immune response keeps cysts from wanting to grow without bounds [56].

Bursting

Parasites contained within a host cell are susceptible to egress through the process of host cell lysis. Eventually, the parasite will cause the cell to burst, infecting the node area with free parasites. These parasites can be in the form of tachyzoites or bradyzoites. The probability of bursting depends on the user-controlled parameter for the maximum threshold for parasites capable of occupying a cell before bursting happens. The probability of a cell bursting increases as the parasite population within a cell approaches the threshold population. The defined rate of bursting is given in Table 6.1. The probability of a host cell infected with tachyzoites bursting is d_T and the probability of a burst for a cell infected with bradyzoites is d_C.

The assumption is made that a host cell dies after parasites contained within cause the cell to burst. Because of the large number of host cells available on an organ, we assume that the birth and death rates of the host cell is the same. Therefore, when a host cell is ruptured, it dies, and a new one is immediately created in the same node.

Inter-conversion

The conversion rate is dependent upon the time that is required for a parasite to convert from tachyzoite to bradyzoite. For each time step, there are two competing processes occurring simultaneously where on one hand the parasites may egress from the host cell, but on the other hand they may convert to a state which has less likelihood of egressing from the host cell. At each time step, there is a probability that a tachyzoite may egress and there is a probability that it may convert to a bradyzoite. If the tachyzoite converts to a bradyzoite, there is a different assigned probability of conversion.

The conversion rate is a probabilistic rule and has a rate of c_{BT} for bradyzoites converting to tachyzoites and c_{TC} for tachyzoites converting to cysted bradyzoites.

If a bradyzoite bursts from a host cell and enters the free space, the free bradyzoite may then invade a new healthy cell. Once the bradyzoite invades, it replicates at the bradyzoite rate. However, the biological process regulates that an invading bradyzoite will eventually convert back in to a tachyzoite [107]. Therefore, there is a separate probability of conversion from bradyzoite to tachyzoite. We also assume that conversion is a synchronous event. For simplicity, the conversion process converts all parasites and does not leave the possibility of observing both types of parasites within the host cell. We also assume conversion is instantaneous in our model.

Survivability of free parasites

In addition to host cell death, free parasites are capable of death when in the intracellular space. Tachyzoites and bradyzoites cannot survive for long times when not inside of a host cell. A free parasite that exists in any free space within a node is capable of dying, staying in the current node, or moving to a new node. Therefore, there exists a chance of a free parasite dying for each time step. This probability is defined as p_d and the numerical value can be seen in Table 6.1.

In the case of free tachyzoites, the probability of death during spreading is a function of the total number of tachyzoites present in the organ:

$$p_{\text{death}} = p_d + (1 - p_d)\,\frac{T_{\text{cf}}}{h_T + K_T} \tag{6.2}$$

where p_d is the probability of a free tachyzoite dying if it is free from a host cell, in absence of immunity, T_{cf} is the number of tachyzoites in the organ, h_T is the attack rate, and K_T is the maximum number of tachyzoites needed before the immune response reaches a maximum rate.

6.2.3 Simulation Techniques

Mesh

This model is developed using mesh generated by the DigiMouse project, which produced a three-dimensional whole-body tetrahedral mesh representation of a mouse [5]. The mesh is created using PET, CT, and cryo-section images. The final result produces 306,773 elements and 58,244 nodes compartmentalized into different organs. The mesh of the brain can be seen in Figure 6.4.

Using the mesh, we use the nodes to represent a region of space where an average number of healthy host cells can exist. We then used random assignment of the number of host cells assigned to each node, which we assume that the spatial heterogeneity of the cells within the organ is preserved in the model. Because this is not a finite element or finite difference problem, the nodes are the only data used in our model and we ignore the element data for simulations.

The mesh is refined using the CubeIt program to increase the number of nodes [33]. The nodes were partitioned into computational nodal-regions through the METIS algorithm [86].

Object-Oriented Programming

The code for the *Toxoplasma gondii* simulation is written in C++. The main objects are represented by the domain of all spatial nodes. Within each primary node object, a secondary object was created to represent each of the cells. Parasites were not represented as an object but as a variable contained within each node and cell. Within each cell, parasites could exist in the tachyzoite state or bradyzoite state. Free parasites can exist within a node and can enter any one of the infected cells. Each cell can only accept one free parasite. Free parasites can exist in tachyzoite, bradyzoite, or an alternate bradyzoite state that can only exist if it has recently come from a burst infected cell, and the alternate bradyzoite's eventually return to the tachyzoite state.

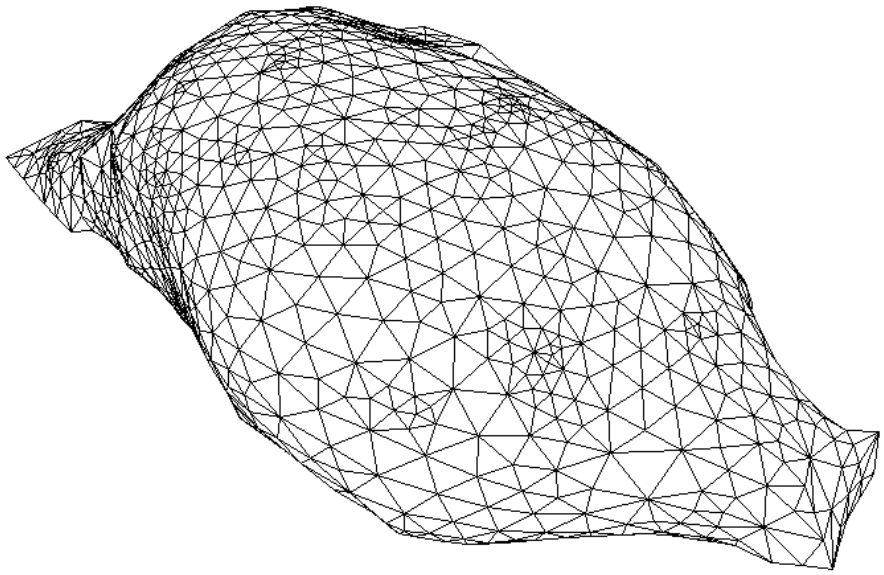

Figure 6.4: Mesh generated from the digitized mouse brain.

Parallelization

The code is written using C++ and implemented in linux on an Intel machine with 8-cores. The code is tested on a multi-processor Linux computer and implemented on the Newton cluster at the University of Tennessee. To implement the code in parallel, Message Passing Interface (MPI) is used to parallelize the algorithms. To parallelize the code, the initial setup is performed in the first processor. The parallelization is done by dividing the brain across the spatial-geographic domain and assigning each region to a separate computation process. After the entire initialization is complete, the first processor sends the node information (location, number of hosts, identification numbers) to each of the secondary processors. Once the simulation begins, the biological rules all apply to each processor simultaneously. The spreading algorithm requires a Send/Receive process through MPI. During the spread process,

the free parasites in one node may to spread to their neighboring nodes. The spreading function is completed by each node retaining a list of neighbors that are within a given neighborhood of the node. If the neighbor is located within a different processor, the free parasite is sent to a buffer node. Once the spreading process is completed in each node, the buffer node sends each of the free parasites to the relevant processor and the parasite enters the node. Once the simulation is complete, the primary processor assembles the data from each processor into a single file for data analysis and visualization.

Algorithm

The code initially reads the mesh, the neighbor lists (generated in pre-processing), and the input parameter choices. A partitioning algorithm is used to assign nodes to different processors. The principal processor sorts the data and sends the appropriate nodal information to each processor. All of the cells are labeled as healthy. An initial dose of 1000 tachyzoites is applied to one node. Discretized time steps of 1 hour are taken and the following process is followed:

- Any free parasites may spread to a neighboring node per the spreading rules. Some free parasites may die in this step.
- Any free parasites may invade a host cell at its new location.
- The parasites that have invaded a host cell may replicate which is a function of the parasite type (bradyzoite or tachyzoite) and a random variable.
- Data is collected and recorded, and time is incremented.

The parameters needed to run this model are based on rates and probabilities found within current literature; see Table 6.1.

Table 6.1: Estimated and experimental parameter estimates used in the simulation.

Paramter	Description	Rate
r_B	Bradyzoite replication rate	1/10 h^{-1}
r_T	Tachyzoite replication rate	1/6 h^{-1}[135]
c_{BT}	Conversion rate from Y_B to Y_T	1/48 h^{-1} [135]
c_{TC}	Conversion rate from Y_T to Y_C conversion	1/20 h^{-1} [81]
d_C	Bradyzoite Bursting Rate	1/(24*30) h^{-1} [123]
d_T	Tachyzoite Bursting Rate	1/8 h^{-1}
N_T	Number of Tachyzoites in host for bursting	8 parasites [55]
N_C	Carrying capacity of Bradyzoites in host	1000 parasites [80]
p_d	Free parasites death rate	0.8 h^{-1}

6.3 Results

To investigate various types of growth functions explored in [124], we simulated the infection with three types of growth for the parasites contained within a cyst: asynchronous growth at the cyst-population level, asynchronous growth at the cyst-parasite level, and synchronous growth at the cyst-population level. This allows us to explore the different hypotheses surrounding the growth behavior of parasites contained within a cyst.

The simulation in this case study was performed assuming that a mouse brain had 10^7 cells, so each node had a random number of cells with a mean of 300. There were 77,221 nodes in the mouse brain mesh. The simulation was carried out using 16 processor nodes. The simulation was evaluated 3600 hours with time steps of 1 hour each. The data was recorded at the end of each time step into a visualization file and a data file, which could then be analyzed.

We investigate three separate replication assumptions. The three separate replication functions are used to generate the distribution of cyst sizes for each hour of the simulation. The plot of infected parasites is shows in Figure 6.6. For a), the synchronous replication rate of tachyzoites shows a large number of small cysts with the potential for much larger cysts. In b), the asynchronous replication rate is modeled

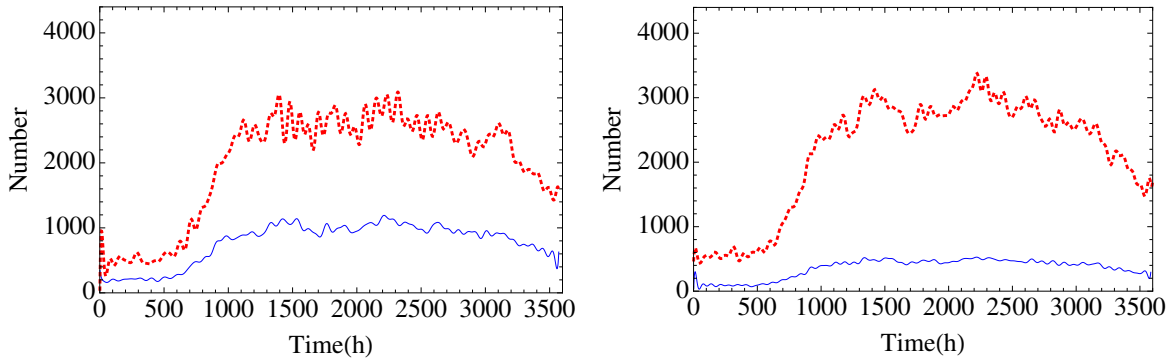

Figure 6.5: Simulation results of one trial. Number of cells infected with tachyzoites and total tachyzoite load (left); number of cells infected with bradyzoites and total bradyzoite load (right).

by introducing a constant number of new cysts for a true probability event. In c), the asynchronous replication is modeled by giving each parasite within a cyst the opportunity to replicate. To test for stationarity, we used the Mann-Whitney median test (selected because the distributions of cyst sizes are not normally distributed)[118]. The test statistic was found by comparing the final simulation hour with each of the previous 100 simulated hours. The results suggested that the medians were not significantly different in at least 99 out of 100 tests at the $\alpha = 0.05$ level for all three growth functions. This allows us to conclude that the distributions have reached stationarity in all three cases.

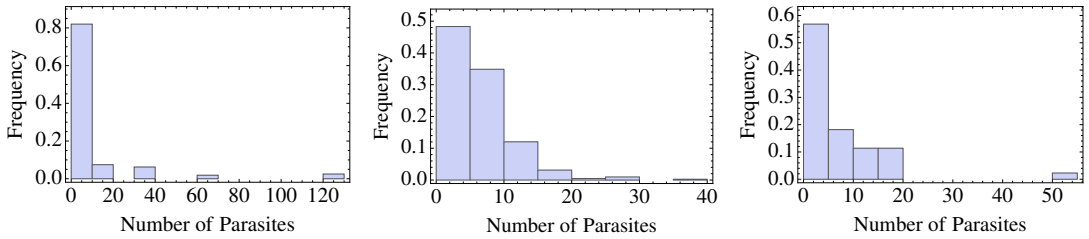

(a) Synchronous replication of a cyst

(b) asynchronous replication of a cyst

(c) Asynchronous replication within a cyst

Figure 6.6: Steady-state cyst-size distributions for different growth functions.

The results shown in Figure 6.5 demonstrate the behavior of the infection of the simulation. During the early period of the infection, cells infected with tachyzoites

begin to appear and persist throughout the early part of the infection. By the end of the first month of infection, the bradyzoites have started to increase in abundance. As the infection carries into the chronic infection stage (3 months or longer), the overall number of cells infected with parasites begins to fall. At this point in the infection, the total number of parasites decreases but the distribution of cyst sizes remains constant.

6.4 Discussion and Conclusion

In this work we developed a cellular automata model to describe the invasion of a *Toxoplasma gondii* within a brain. The model was developed using the mechanistic life cycle models to simulate the parasitic invasion on a mouse brain. The invasion, replication, stage-conversion, and egress processes were modeled according to realistic experimental parameters. The results of the model were presented to explore three different growth processes for bradyzoite replication. The steady-state distributions were explored to examine the behavior of the distributions as chronic infection developed. Finally, a variety of tools were used to display the output of the model as plots and 3D models.

The data collected for each time step allows for observing healthy cells, cells infected with bradyzoites, tachyzoites, or secondary bradyzoites, and free tachyzoites and bradyzoites. There are also data collected to describe the number of each type of parasite found within host cells.

In exploring the 3 separate growth functions, the trends observed are supported by the findings of the partial differential equation model developed for the cyst volume growth in Sullivan et.al. [124]. In that model, they proposed that the growth rate could be constant (asynchronous), linear increasing (synchronous), or logistic. In the model observations, the synchronous models followed a negative exponential function with a coefficient in the exponent that forced the function to go to 0 much too quickly compared to the distribution of the data. However, their model showed that the

constant growth rate function was able to fit the data the best. In our observations of the model in Figure 6.6, the asynchronous growth at the cyst level appears to closely resembles the distribution of data observed in the experiments performed in [124] at steady state.

The target audience of this model is biologists who need a convenient way to test parameters and outcomes from infection in mice. By using this model, biologists may be able to determine replication and conversion rates by looking at existing data from within their experiments. This model could be used to examine different strain types along with various effects of initial dosages and compared to experimental data. For example, the data collected in Mordue et. al. [104] demonstrates the parasite load on various organs as well as the effect of mortality caused by varying strain types.

Future work on this model would allow for simulating the transmission of the parasite over the entire mouse body. The immune system modeling would need to be examined such that the immune response would transmit the parasites from organ to organ. The transmission and reproductive rates, along with the immune system response, might be difficult to determine for each organ. An updated immune system modeling technique may also be needed to more accurately represent the various methods of immunity response.

Overall, this tool has proven useful in observing trends found on mechanistic ODE models and PDE models. Additionally, the findings of this model are generally in support of experimental observations of *Toxoplasma gondii*. Specifically, the convergence of the model to a steady-state, along with the observation that the asynchronous growth at the cyst level shows similar behavior to previous models and data demonstrates the validity of the assumptions made in our model.

Chapter 7

Conclusions

Here we have presented a multitude of modeling techniques applied to the unique life-cycle of *T. gondii*. As demonstrated, there are unique aspects of the acute infection cycle, chronic infection stage, and other biological phenomenon observable when viewing the entire life cycle. In the development of the various models presented here, the use of real experimental data provides additional support to the models developed here. Finally, we used a variety of dynamic and statistical processes to analyze and make conclusions based upon our developed models.

The work presented here was unique in that there have not been models designed to describe the complete life cycle of *T. gondii* infection to this degree. Further, the use of real experimental data to validate various modeling assumptions allows us to make stronger conclusions than if the models had been developed on a purely theoretical basis.

For the acute infection model, 16 nested models were developed with different assumptions. Each of the 16 models were fit to existing experimental data from the brains of mice. The relative "fit" of the models was compared using the DIC. It was interesting that despite being penalized for having more effective parameters, the model that best described the data was the model that had two state of immune response and two states of parasite. Therefore, the significant conclusion from the

acute infection model is that parasites undergo an initial infection state and the immune response has a primed and active state despite typically only observing a single state experimentally.

In the chronic infection analysis, multiple models were compared using the AIC for model selection. In particular, multiple growth and removal functions were considered. The experimental data did not support any growth function except the constant growth rate function. This is interesting because the typically dividing parasites or cells are typically thought to divide according to a linear growth rate function. This finding is significant because it suggests that parasites within a cyst produce offspring as a community of parasites contained within the cyst, and not necessarily as individuals. Despite the various removal functions, it was difficult to differentiate the models with the best AIC values.

The within-host dynamics theoretical model attempted to combine the acute infection process and the chronic infection process by introducing a stage-conversion process. This model analyzed the dynamics of the parasitic infection within a host. The analysis of the dynamics of this model suggest that there are 3 distinct equilibrium: a disease-free equilibrium, an immune-free endemic equilibrium, and an immune-response mediated endemic equilibrium. It is interesting to note that the parasites are capable of persisting at equilibrium levels while never triggering an immune response. The numerical simulations of the model were also presented where the host suffers a temporary reduction in immune response. Despite the reduction in immune response, the model demonstrated that the host was able to quickly recover to nearly identical levels once the host immune response recovered.

Finally, the cellular automata model used probabilistic rules to demonstrate the acute and chronic infection of the parasites infecting a brain. The model investigated the various growth mechanisms and reproduced the overall trends observed in the chronic infection model for the growth behavior. The model incorporated a wide-range of biological assumptions and the output of the steady-state histogram showed validated the assumptions when compared to experimental data. While this toolbox

used parameters found in the literature as compared to finding parameters via statistical methods, the behavior of the model is supported by other models in this project and the experimental data.

As a recommendation for future work, there are three main areas that I would like to see investigated. Firstly, these models are general in the sense that they are applied to a nonvirulent strain of parasite. It would be interesting to develop a more stringent model that would predict mortality or account for more virulent strain types. To fulfill the modeling strategies used in this model, it would be necessary to collect data using the more virulent strains of *Toxoplasma gondii*. It would also be possible to include additional mortality terms defined in the model to describe when a host would be susceptible to death.

As a second goal in future work, it would be interesting to further develop the cellular automata model in such a way that the infection would spread from organ to organ. In the mesh file that was used, the different organs that are susceptible to parasitic infection could be used to host the infection in addition to the brain. For example, the parasite could begin spreading in the intestines and spread to the spleen, liver, etc. Finally, the parasite could make its way to the brain. It would be interesting because many of the transport mechanisms would need to be modeled. This model could be used to compare to data found for the entire host infection over a period of time.

Finally, additional data could be used to strengthen the conclusions found from these models. An experimental design that incorporated the chronic and acute infection scale could be used to develop a parameter estimating routine for the within-host dynamics model. Additionally, an experiment that more accurately captured the organ-specific IFN-γ levels and parasite densities would be helpful in further strengthening the conclusions of the model. For the chronic infection model, using a high-throughput method to collect data and find small cysts that may have been ignored with a manual counting method would provide a better data set to match

models to. Having cyst distributions at daily or weekly intervals would allow for model fitting of the transients in addition to the steady-state.

Bibliography

[1] Avian influenza optimal seasonal vaccination strategy. *The Anziam Journal*, 51:394–405, 2010. 57

[2] Modeling toxoplasmosis spread in cat populations under vaccination. *Theoretical Population Biology*, 77:227–237, 2010. 44

[3] Theoretical assessment of avian influenza vaccine. *DCDS Series B*, 13(1):1 – 25, 2010. 54

[4] Toxoplasmosis, November 2010. `http://www.cdc.gov/toxoplasmosis/`. 2, 7, 8, 65, 66

[5] Biomedical imaging research lab, January 2011. `http://neuroimage.usc.edu/Digimouse.html`. 73

[6] D. Ajzenberg, N. Cogn, L. Paris, M. Bessires, P. Thulliez, D. Filisetti, H. Pelloux, P. Marty, and M. Dard. Genotype of 86 toxoplasma gondii isolates associated with human congenital toxoplasmosis, and correlation with clinical findings. *Journal of Infectious Diseases*, 186(5):684–689, 2002. 32

[7] Hirotugu Akaike. A bayesian analysis of the minimum aic procedure. *Annals of the Institute of Statistical Mathematics*, 30:9–14, 1978. 10.1007/BF02480194. 17

[8] D. Aldebert, M. Hypolite, P. Cavailles, B. Touquet, P. Flori, C. Loeuillet, and M. F. Cesbron-Delauw. Development of High-Throughput Methods to Quantify Cysts of Toxoplasma gondii. *CYTOMETRY PART A*, 79A(11):952–958, NOV 2011. 9, 43

[9] R. M. Anderson and R May. *Infectious Diseases of Humans*. Oxford University Press, New York., 1991. 52

[10] R. M. Anderson and R. M. May. Coevolution of hosts and parasites. *Parasitology*, 85(02):411–426, 1982. 11

[11] R.M. Anderson and R.M. May. Population biology of infectious diseases: Part I. *Nature*, 280:361–367, 1979. 11, 12, 13, 14

[12] G. Arrizabalaga, F. Ruiz, S. Moreno, and J. C. Boothroyd. Ionophore-resistant mutant of Toxoplasma gondii reveals involvement of a sodium/hydrogen exchanger in calcium regulation. *J. Cell Biol.*, 165(5):653–662, Jun 2004. 20

[13] Mylene Bedard. Optimal acceptance rates for Metropolis algorithms: Movin beyond 0.234. *Stochastic Processes and Their Applications*, 118(12):2198–2222, DEC 2008. 28

[14] M. Berdoy, J. P. Webster, and D. W. Macdonald. Fatal attraction in rats infected with toxoplasma gondii. *Proceedings of the Royal Society of London. Series B: Biological Sciences*, 267(1452):1591–1594, 2000. 2

[15] Miroslava Berenreiterova, Jaroslav Flegr, Ales A. Kubena, and Pavel Nemec. The Distribution of Toxoplasma gondii Cysts in the Brain of a Mouse with Latent Toxoplasmosis: Implications for the Behavioral Manipulation Hypothesis. *PLOS ONE*, 6(12), DEC 14 2011. 9

[16] A Berg, R Meyer, and J Yu. Deviance information criterion for comparing stochastic volatility models. *Journal of Business & Economic Statistics*, 22(1):107–120, JAN 2004. 28

[17] Andreas Berg, Renate Meyer, and Jun Yu. Deviance information criterion for comparing stochastic volatility models. *Journal of Business and Economic Statistics*, 22:107–119, 2002. 18, 19

[18] L. T. Biegler, J. J. Damiano, and G. E. Blau. Nonlinear parameter estimation: A case study comparison. *AIChE Journal*, 32(1):29–45, 1986. 16

[19] Michael W. Black and John C. Boothroyd. Lytic cycle of toxoplasma gondii. *Microbiology and Molecular Biology Reviews*, 64(3):607–623, 2000. 8, 20

[20] S. K. Bliss, A. J. Marshall, Y. Zhang, and E. Y. Denkers. Human polymorphonuclear leukocytes produce IL-12, TNF-alpha, and the chemokines macrophage-inflammatory protein-1 alpha and -1 beta in response to Toxoplasma gondii antigens. *J. Immunol.*, 162(12):7369–7375, Jun 1999. 21

[21] R.J. De Boer and A.S. Perelson. Target cell limited and immune control models of hiv infection: A comparison. *Journal of Theoretical Biology*, 190(3):201 – 214, 1998. 11

[22] B.M. Bolker. *Ecological models and data in R.* Princeton University Press, Princeton, NJ, 2008. 16, 18

[23] Hamparsum Bozdogan. Model selection and akaike's information criterion (aic): The general theory and its analytical extensions. *Psychometrika*, 52:345–370, 1987. 10.1007/BF02294361. 17

[24] F Brauer and C Castillo-Chavez. *Mathematical models in population biology and epidemiology.* Springer, 2001. 47

[25] Fred Brauer and P. van den Driessche. Models for transmission of disease with immigration of infectives. *Mathematical Biosciences*, 171(2):143 – 154, 2001. 57

[26] J. Burkhart. Mathematica markov chain monte carlo routine. `http://astro.berkeley.edu/~burkart/code.html`, August 2012. 27

[27] P. Burnah and D. Anderson. *Model Selection and Multimodel Inference.* Springer, 2002. 16, 17, 40

[28] Angel Calsina and Joan Saldana. A model of physiologically structured population dynamics with a nonlinear individual growth rate. *Journal of Mathematical Biology*, 33:335–364, 1995. 10.1007/BF00176377. 35

[29] Vern B. Carruthers. Host cell invasion by the opportunistic pathogen toxoplasma gondii. *Acta Tropica*, 81(2):111 – 122, 2002. 8

[30] Liujuan Chen, Fengde Chen, and Lijuan Chen. Qualitative analysis of a predator-prey model with holling type ii functional response incorporating a constant prey refuge. *Nonlinear Analysis: Real World Applications*, 11(1):246 – 252, 2010. 48

[31] Daniel Coombs, Michael A. Gilchrist, and Colleen L. Ball. Evaluating the importance of within- and between-host selection pressures on the evolution of chronic pathogens. *Theoretical Population Biology*, 72(4):576 – 591, 2007. 11

[32] I. Coppens, J. D. Dunn, J. D. Romano, M. Pypaert, H. Zhang, J. C. Boothroyd, and K. A. Joiner. Toxoplasma gondii sequesters lysosomes from mammalian hosts in the vacuolar space. *Cell*, 125(2):261–274, Apr 2006. 21

[33] CubeIt. *version 13.1*. Sandia National Lab, Albuquerque, NM, 2011. 73

[34] J. M. Cushing. *An Introduction to Structured Population Dynamics*. SIAM, Philiadelphia, 1998. 35

[35] Marialice da Fonseca Ferreira-da Silva, Anna C. Takcs, Helene S. Barbosa, Uwe Gross, and Carsten G.K. Lder. Primary skeletal muscle cells trigger spontaneous toxoplasma gondii tachyzoite-to-bradyzoite conversion at higher rates than fibroblasts. *International Journal of Medical Microbiology*, 299(5):381 – 388, 2009. 60

[36] Rodrigo C. da Silva, Aristeu V. da Silva, and Helio Langoni. Recrudescence of Toxoplasma gondii infection in chronically infected rats (Rattus norvegicus). *Experimental Parasitology*, 125(4):409–412, AUG 2010. 61

[37] M. L. Darde, B. Bouteille, and M. Pestre-Alexandre. Isoenzyme analysis of 35 Toxoplasma gondii isolates and the biological and epidemiological implications. *J. Parasitol.*, 78(5):786–794, Oct 1992. 32

[38] M. H. DeGroot and M. J. Schervish. *Probability and Statistics*. Addison-Wesley, London, 2002. 40

[39] E. Y. Denkers. Toll-like receptor initiated host defense against Toxoplasma gondii. *J. Biomed. Biotechnol.*, 2010:737125, 2010. 21

[40] Manlio Di Cristian, Daniela Marocco, Roberto Galizi, Carla Proietti, Roberta Spaccapelo, and Andrea Crisanti. Temporal and spatial distribution of Toxoplasma gondii differentiation into bradyzoites and tissue cyst formation in vivo. *INFECTION AND IMMUNITY*, 76(8):3491–3501, AUG 2008. 9

[41] U. Dieckmann, J.A.J. Metz, M.W. Sabelis, and K. Sigmund. *Adaptive Dynamics of Infectious Diseases*. Cambridge, 2002. 14

[42] O. Diekmann, M. Gyllenberg, H. Huang, M. Kirkilionis, J.A.J. Metz, and H.R. Thieme. On the formulation and analysis of general deterministic structured population models ii. nonlinear theory. *Journal of Mathematical Biology*, 43:157–189, 2001. 10.1007/s002850170002. 25

[43] O. Diekmann and J.A.P Heesterbeek. *Mathematical Epidemiology of Infectious Diseases*. Wiley, 2000. 14

[44] O Diekmann, JAP Heesterbeek, and JAP Metz. On the definition and computation of the basic reproduction ratio r_0 in models for infectious diseases in heterogeneous populations. *J. Math. Biol.*, 28:503–522, 1990. 52

[45] Ferguson DJ. Toxoplasma gondii and sex: Essential or optional extra? *Trends Parasito*, 18:355–359, 2009. xi, 45

[46] J. M. Dobrowolski and L. D. Sibley. Toxoplasma invasion of mammalian cells is powered by the actin cytoskeleton of the parasite. *Cell*, 84(6):933–939, Mar 1996. 20

[47] J. P. Dubey, D. S. Lindsay, and C. A. Speer. Structures of toxoplasma gondii tachyzoites, bradyzoites, and sporozoites and biology and development of tissue cysts. *Clin. Microbiol. Rev.*, 11(2):267–299, 1998. 1, 7, 8, 60

[48] J.P. Dubey. *Toxoplasmosis of Animals and Humans*. CRC Press, 2010. 44, 45, 48, 58, 59, 63

[49] I. R. Dunay, R. A. Damatta, B. Fux, R. Presti, S. Greco, M. Colonna, and L. D. Sibley. Gr1(+) inflammatory monocytes are required for mucosal resistance to the pathogen Toxoplasma gondii. *Immunity*, 29(2):306–317, Aug 2008. 1, 20, 21

[50] I. R. Dunay, A. Fuchs, and L. D. Sibley. Inflammatory monocytes but not neutrophils are necessary to control infection with Toxoplasma gondii in mice. *Infect. Immun.*, 78(4):1564–1570, Apr 2010. 21

[51] I. R. Dunay and L. D. Sibley. Monocytes mediate mucosal immunity to Toxoplasma gondii. *Curr. Opin. Immunol.*, 22(4):461–466, Aug 2010. 1, 20

[52] Lourdes Esteva, Abba B. Gumel, and Cruz Vargas de Lean. Qualitative study of transmission dynamics of drug-resistant malaria. *Mathematical and Computer Modelling*, 50:611 – 630, 2009. 54

[53] G.J.D. Smith *et al.* Emergence and predominance of an h5n1 influenza variant in china. *Proc. Natl. Acad. Sci. U.S.A.*, 103:16936–16941., 2006. 53

[54] Jozsef Z. Farkas and Thomas Hagen. Linear stability and positivity results for a generalized size-structured Daphnia model with inflow. *APPLICABLE ANALYSIS*, 86(9):1087–1103, 2007. 15

[55] M. d. a. F. Ferreira-da Silva, A. C. Takacs, H. S. Barbosa, U. Gross, and C. G. Luder. Primary skeletal muscle cells trigger spontaneous Toxoplasma gondii tachyzoite-to-bradyzoite conversion at higher rates than fibroblasts. *Int. J. Med. Microbiol.*, 299(5):381–388, Jun 2009. 76

[56] Denis Filisetti and Ermanno Candolfi. Immune response to toxoplasma gondii. *Ann Ist Super Sanita*, 40(1):71 – 80, 2004. 47, 71

[57] A. Freyre, J. Falcn, J. Mendez, and M. Gonzlez. Toxoplasma gondii: Differential protection rates by two strains against cyst formation in a rat model. *Experimental Parasitology*, 114(4):265 – 270, 2006. 10

[58] S. M. Garba and A. B. Gumel. Effect of cross-immunity on the transmission dynamics of two strains of dengue. *Int. J. Comput. Math.*, 87(10):2361–2384, August 2010. 54

[59] S.M. Garba, A.B. Gumel, and M.R. Abu Bakar. Backward bifurcations in dengue transmission dynamics. *Mathematical Biosciences*, 215(1):11 – 25, 2008. 54

[60] R Gazzinelli, Y Xu, S Hieny, A Cheever, and A Sher. Simultaneous depletion of cd4+ and cd8+ t lymphocytes is required to reactivate chronic infection with toxoplasma gondii. *The Journal of Immunology*, 149(1):175–80, 1992. 1

[61] R. Gazzinelli, Y. Xu, S. Hieny, A. Cheever, and A. Sher. Simultaneous depletion of CD4+ and CD8+ T lymphocytes is required to reactivate chronic infection with Toxoplasma gondii. *J. Immunol.*, 149(1):175–180, Jul 1992. 21

[62] MICHAEL A. GILCHRIST and AKIRA SASAKI. Modeling hostparasite coevolution: A nested approach based on mechanistic models. *Journal of Theoretical Biology*, 218(3):289 – 308, 2002. 11

[63] Gilberto C. Gonzlez-Parra, Abraham J. Arenas, Diego F. Aranda, Rafael J. Villanueva, and Lucas Jadar. Dynamics of a model of toxoplasmosis disease in human and cat populations. *Computers & Mathematics with Applications*, 57(10):1692 – 1700, 2009. 44

[64] M. E. Grigg, S. Bonnefoy, A. B. Hehl, Y. Suzuki, and J. C. Boothroyd. Success and virulence in Toxoplasma as the result of sexual recombination between two distinct ancestries. *Science*, 294(5540):161–165, Oct 2001. 32

[65] Marc-Jan Gubbels. Toxoplasma gondii, April 2011. x, xii, 10, 66

[66] A. B. Gumel. Global dynamics of a two-strain avian influenza model. *Int. J. Comput. Math.*, 86(1):85–108, January 2009. 54

[67] W. K. Hastings. Monte carlo sampling methods using markov chains and their applications. *Biometrika*, 57(1):97–109, 1970. 26

[68] H. W. Hethcote. The mathematics of infectious diseases. *SIAM Rev*, 42(4):599–653, 2000. 52

[69] R. Hilborn and M. Mangel. *The Ecological Detective*. Princeton University Press, Princeton, NJ, 1997. 17

[70] M. E. Hochberg, M. P. Hassell, and R. M. May. The dynamics of host-parasitoid-pathogen interactions. *The American Naturalist*, 135(1):pp. 74–94, 1990. 11

[71] R.E. Holliman. Toxoplasmosis, behaviour and personality. *Journal of Infection*, 35(2):105 – 110, 1997. 2

[72] Hossein Hooshyar, Parvin Rostamkhani, and Mohsen Arbabi. Study on growth of toxoplasma gondii tissue cyst in laboratory mouse. *Jundishapur Joural of Microbiology*, 2(4):140–143, 2009. 39, 40

[73] D. K. Howe and L. D. Sibley. Toxoplasma gondii comprises three clonal lineages: correlation of parasite genotype with human disease. *J. Infect. Dis.*, 172(6):1561–1566, Dec 1995. 32

[74] S.S. Jang and R.B. Gopaluni. Parameter estimation in nonlinear chemical and biological processes with unmeasured variables from small data sets. *Chemical Engineering Science*, 66(12):2774 – 2787, 2011. 27

[75] C. Jeffries, V. Klee, and P. Van Den Driessch. When is a Matrix Sign Stable? *Can J. Math*, 29(2):315–326, 1977. 57

[76] M. E. JEROME, J. R. RADKE, W. BOHNE, D. S. ROOS, and M. W. WHITE. Toxoplasma gondii bradyzoites form spontaneously during sporozoite-initiated development. *INFECTION AND IMMUNITY*, 66:48384844, 1998. 48

[77] W. Jiang, A.M. Sullivan, C. Su, and X. Zhao. An agent-based model for the transmission dynamics of *Toxoplasma gondii*. *Journal of Theoretical Biology*, 293(0):15 – 26, 2012. 7, 33

[78] Wen Jiang, Adam M. Sullivan, Chunlei Su, and Xiaopeng Zhao. An agent-based model for the transmission dynamics of toxoplasma gondii. *Journal of Theoretical Biology*, 293(0):15 – 26, 2012. 44

[79] Jerald B. Johnson and Kristian S. Omland. Model selection in ecology and evolution. *Trends in Ecology & Evolution*, 19(2):101 – 108, 2004. 40

[80] Dubey JP. *Toxoplasmosis of Animals and Humans*. CRC Press, 2009. 65, 67, 76

[81] JR Radke JR, RG Donald, A Eibs, ME Jerome, MS Behnke, P Liberator, and WW White. Changes in the expression of the human cell division autoantigen-1 influence toxoplasma gondii growth and development. *PLoS Pathog.*, 2:105, 2006. 60, 76

[82] B. F. Kafsack, J. D. Pena, I. Coppens, S. Ravindran, J. C. Boothroyd, and V. B. Carruthers. Rapid membrane disruption by a perforin-like protein facilitates parasite exit from host cells. *Science*, 323(5913):530–533, Jan 2009. 20

[83] Bjorn F.C. Kafsack, Vern B. Carruthers, and Fernando J. Pineda. Kinetic modeling of toxoplasma gondii invasion. *Journal of Theoretical Biology*, 249:817825, 2007. 48

[84] H. Kang and Y. Suzuki. Requirement of non-T cells that produce gamma interferon for prevention of reactivation of Toxoplasma gondii infection in the brain. *Infect. Immun.*, 69(5):2920–2927, May 2001. 32

[85] A. R. KANSAL, S. TORQUATO, G. R. HARSH, E. A. CHIOCCA, and T. S. DEISBOECK. Simulated brain tumor growth dynamics using a three-dimensional cellular automaton. *Journal of Theoretical Biology*, 203(4):367 – 382, 2000. 70

[86] G. Karypis and V Kumar. A fast and highly quality multilevel scheme for partitioning irregular graphs. *SIAM Journal on Scientific Computing*, 20(1):359–392, 1999. 73

[87] MJ Keeling and P Rohani. *Modeling Infectious Diseases in Humans and Animals*. Princeton Press, 2008. 47

[88] W. O. Kermack and A. G. McKendrick. Contributions to the mathematical theory of epidemics. ii. the problem of endemicity. *Proceedings of the Royal Society of London. Series A, Containing Papers of a Mathematical and Physical Character*, 138(834):pp. 55–83, 1932. 14

[89] Benjamin C Kuo and M Farid Golnaraghi. *Automatic control systems*. John Wiley & Sons New York, 2003. 25

[90] V. Lakshmikantham, S. Leela, and A.A. Martynyuk. *Stability Analysis of Nonlinear Systems*. Marcel Dekker, Inc., New York and Basel., 1989. 53

[91] P.H.L. LAMBERTON, C.A. DONNELLY, and J.P. WEBSTER. Specificity of the toxoplasma gondii-altered behaviour to definitive versus non-definitive host predation risk. *Parasitology*, 135:1143–1150, 8 2008. 2

[92] M. Langlais, M. Llu, C. Avenet, and E. Gilot-Fromont. A simplified model system for toxoplasma gondii spread within a heterogeneous environment. *Nonlinear Dynamics*, 68:381–399, 2012. 14

[93] M Lelu, M Langlais, ML Poulle, and E Gilot-Fremont. Transmission dynamics of toxoplasma gondii along an urban-rural gradient. *Theoretical Population Biology*, 78:139–147, 2010. 14

[94] Leandro Lemgruber, Pietro Lupetti, Erica S. Martins-Duarte, Wanderley De Souza, and Rossiane C. Vommaro. The organization of the wall filaments and characterization of the matrix structures of Toxoplasma gondii cyst form. *CELLULAR MICROBIOLOGY*, 13(12):1920–1932, DEC 2011. 8, 9

[95] S. Luo, M. Reed, J. C. Mattingly, and K. Koelle. The impact of host immune status on the within-host and population dynamics of antigenic immune escape. *Journal of The Royal Society Interface*, 9(75):2603–2613, 2012. 23

[96] Kot M. *Elements of Mathematical Ecology.* Cambridge University Press, 2003. 12, 14, 48

[97] J. D. MacMicking. Interferon-inducible effector mechanisms in cell-autonomous immunity. *Nat. Rev. Immunol.*, 12(5):367–382, May 2012. 21

[98] M. Mashayekhi, M. M. Sandau, I. R. Dunay, E. M. Frickel, A. Khan, R. S. Goldszmid, A. Sher, H. L. Ploegh, T. L. Murphy, L. D. Sibley, and K. M. Murphy. CD8(+) dendritic cells are the critical source of interleukin-12 that controls acute infection by Toxoplasma gondii tachyzoites. *Immunity*, 35(2):249–259, Aug 2011. 21

[99] T. C. Melzer, H. J. Cranston, L. M. Weiss, and S. K. Halonen. Host cell preference of toxoplasma gondii cysts in murine brain: A confocal study. *J Neuroparasitology*, 1, 2010. 39

[100] N. Metropolis, A. W. Rosenbluth, M. N. Rosenbluth, A. H. Teller, and E. Teller. Equation of state calculations by fast computing machines. *The Journal of Chemical Physics*, 21(6):1087–1092, 1953. 26

[101] D. G. Mordue, S. Hakansson, I. Niesman, and L. D. Sibley. Toxoplasma gondii resides in a vacuole that avoids fusion with host cell endocytic and exocytic vesicular trafficking pathways. *Exp. Parasitol.*, 92(2):87–99, Jun 1999. 21

[102] D. G. Mordue and L. D. Sibley. Intracellular fate of vacuoles containing Toxoplasma gondii is determined at the time of formation and depends on the mechanism of entry. *J. Immunol.*, 159(9):4452–4459, Nov 1997. 21

[103] D. G. Mordue and L. D. Sibley. A novel population of Gr-1+-activated macrophages induced during acute toxoplasmosis. *J. Leukoc. Biol.*, 74(6):1015–1025, Dec 2003. 1, 20, 21

[104] Dana G. Mordue, Fernando Monroy, Marie La Regina, Charles A. Dinarello, and L. David Sibley. Acute toxoplasmosis leads to lethal overproduction of th1 cytokines. *The Journal of Immunology*, 167(8):4574–4584, 2001. 26, 28, 29, 31, 79

[105] JD Murray. *Mathematical Biology I: An Introduction*. Springer, 2002. 47

[106] M.A. Nowak and R.M. May. *Virus Dynamics: Mathematical Principles of Immunology and Virology*. Oxford University Press, 2000. 47

[107] H Odaert, M Soete, B Fortier, and D Camus. Stage conversion of toxoplasma gondii in mouse brain during infection and immunodepression. *Parasitol Res*, 82:28 – 31, 1996. 72

[108] D. Oldfield. A continuity equation for cell populations. *Bulletin of Mathematical Biology*, 28:545–554, 1966. 10.1007/BF02476861. 15

[109] Kasia A. Pawelek, Giao T. Huynh, Michelle Quinlivan, Ann Cullinane, Libin Rong, and Alan S. Perelson. Modeling within-host dynamics of influenza virus infection including immune responses. *PLoS Comput Biol*, 8(6):e1002588, 06 2012. 11

[110] Carolina Pina-Vazquez, Rafael Saavedra, and Pascal Herion. A quantitative competitive PCR method to determine the parasite load in the brain of Toxoplasma gondii-infected mice. *PARASITOLOGY INTERNATIONAL*, 57(3):347–353, SEP 2008. 9, 39

[111] Katharine F Preedy, Piet G Schofield, Mark A.J Chaplain, and Stephen F Hubbard. Disease induced dynamics in hostparasitoid systems: chaos and coexistence. *Journal of The Royal Society Interface*, 4(14):463–471, 2007. 11

[112] P. M. Robben, M. LaRegina, W. A. Kuziel, and L. D. Sibley. Recruitment of Gr-1+ monocytes is essential for control of acute toxoplasmosis. *J. Exp. Med.*, 201(11):1761–1769, Jun 2005. 21

[113] P. M. Robben, D. G. Mordue, S. M. Truscott, K. Takeda, S. Akira, and L. D. Sibley. Production of IL-12 by macrophages infected with Toxoplasma gondii depends on the parasite genotype. *J. Immunol.*, 172(6):3686–3694, Mar 2004. 21

[114] C.P. Robert and G. Casella. *Introducing Monte Carlo Methods with R*. Springer, 2010. 18

[115] T. M. Scharton-Kersten, G. Yap, J. Magram, and A. Sher. Inducible nitric oxide is essential for host control of persistent but not acute infection with the intracellular pathogen Toxoplasma gondii. *J. Exp. Med.*, 185(7):1261–1273, Apr 1997. 21

[116] O. Sharomi and A.B. Gumel. Re-infection-induced backward bifurcation in the transmission dynamics of chlamydia trachomatis. *Journal of Mathematical Analysis and Applications*, 356(1):96 – 118, 2009. 54

[117] O. Sharomi, C. N. Podder, A. B. Gumel, and B. Song. Mathematical analysis of the transmission dynamics of HIV/TB coinfection in the presence of treatment. *Math Biosci Eng*, 5(1):145–174, Jan 2008. 54

[118] Galen R Shorack and Nhu D Le. Modification of the mann-whitney test. *Journal of Statistical Computation and Simulation*, 31(1):9–17, 1989. 77

[119] J. W. Sinko and W. Streifer. A new model for age-size structure of a population. *Ecology*, 48(6):910–916, 1967. 15, 34

[120] Garrick Skalski and James Gilliam. Functional responses with predator interference: Viable alternatives to the holling type ii model. *Ecology*, 82(11):3083 – 3092, 2001. 48

[121] Sini Skariah, Matthew McIntyre, and Dana Mordue. Toxoplasma gondii determinants of tachyzoite to bradyzoite conversion. *Parasitology Research*, 107:253–260, 2010. 10.1007/s00436-010-1899-6. 9, 70

[122] I. C. Ster and N. M. Ferguson. Transmission parameters of the 2001 foot and mouth epidemic in great britain. *PLoS One*, 2(6), JUN 2007. 28

[123] A. Sullivan, F. Agusto, S. Bewick, C. Su, S. Lenhart, and X. Zhao. A mathematical model for within-host *Toxoplasma gondii* invasion dynamics. *Mathematical Biosciences and Engineering*, 9(3):647–662, 2012. xii, 22, 33, 45, 69, 76

[124] A. Sullivan, X. Zhao, Y. Suzuki, E. Ochaii, S. Crutcher, and M. Gilchrist. Evidence of asynchronous growth of toxoplasma gondii cysts based on data-driven model selection. *Submitted.*, 2013. 76, 78, 79

[125] A.M. Sullivan, X. Zhao, Y. Suzuki, Eri Ochiai, Stephen Crutcher, and M.A. Gilchrist. Evidence of asynchronous growth of toxoplasma gondii cyst based on data-driven model selection. submitted. 22

[126] E. Suss-Toby, J. Zimmerberg, and G. E. Ward. Toxoplasma invasion: the parasitophorous vacuole is formed from host cell plasma membrane and pinches off via a fission pore. *Proc. Natl. Acad. Sci. U.S.A.*, 93(16):8413–8418, Aug 1996. 21

[127] Y. Suzuki, F. K. Conley, and J. S. Remington. Importance of endogenous IFN-gamma for prevention of toxoplasmic encephalitis in mice. *J. Immunol.*, 143(6):2045–2050, Sep 1989. 21

[128] Y Suzuki, MA Orellana, RD Schreiber, and JS Remington. Interferon-gamma: the major mediator of resistance against toxoplasma gondii. *Science*, 240(4851):516–518, 1988. 21

[129] Yasuhiro Suzuki, Qila Sa, Marie Gehman, and Eri Ochiai. Interferon-gamma- and perforin-mediated immune responses for resistance against toxoplasma gondii in the brain. *Expert Reviews in Molecular Medicine*, 13:null–null, 2011. 9

[130] Yasuhiro Suzuki, Xisheng Wang, Benard S. Jortner, Laura Payne, Yanyan Ni, Sara A. Michie, Baohui Xu, Tomoya Kudo, and Sara Perkins. Removal of toxoplasma gondii cysts from the brain by perforin-mediated activity of cd8+ t cells. *The American Journal of Pathology*, 176(4):1607 – 1613, 2010. 32

[131] Yasuhiro Takashima, Kazuhiko Suzuki, Xuenan Xuan, Yoshifumi Nishikawa, Akihiro Unno, and Katsuya Kitoh. Detection of the initial site of toxoplasma gondii reactivation in brain tissue. *International Journal for Parasitology*, 38(5):601 – 607, 2008. 9

[132] Iauw Bhieng Tjoa and Lorenz T. Biegler. Simultaneous solution and optimization strategies for parameter estimation of differential-algebraic equation systems. *Industrial & Engineering Chemistry Research*, 30(2):376–385, 1991. 16

[133] P. van den Driessche and J. Watmough. Reproduction numbers and sub-threshold endemic equilibria for compartmental models of disease transmission. *Math. Biosci.*, 180:29–48, 2002. 51, 52, 53

[134] Joanne P. Webster. The effect of toxoplasma gondii on animal behavior: Playing cat and mouse. *Schizophrenia Bulletin*, 33(3):752–756, 2007. 2

[135] Louis Weiss and Kami Kim. *Toxoplasma gondii*. Academic Press, 2007. 48, 60, 76

[136] Wikipedia. File:toxoplasmosis life cycle en.svg, 2013. [Online; accessed: 30-April-2013]. x, 3

[137] D Wodarz. *Killer Cell Dynamics: Mathematical and Computational Approaches to Immunology*. Springer, 2007. 47, 48

[138] Inc. Wolfram Research. *Mathematica Edition: Version 8.0*. Wolfram Research, Inc., Champaign, Illinois, 2010. 27

[139] G. S. Yap and A. Sher. Effector cells of both nonhemopoietic and hemopoietic origin are required for interferon (IFN)-gamma- and tumor necrosis factor (TNF)-alpha-dependent host resistance to the intracellular pathogen, Toxoplasma gondii. *J. Exp. Med.*, 189(7):1083–1092, Apr 1999. 21

[140] G Zuur, PH Garthwaite, and RJ Fryer. Practical use of MCMC methods: Lessons from a case study. *Biometrical Journal*, 44(4):433–455, 2002. 28

Vita

Adam Sullivan was born in Pittsburgh, PA, USA, on February 11, 1987. After finishing high-school in 2005 at Brashear High School in Pittsburgh, he attended Edinboro University of PA in Edinboro, PA. He graduated in 2009 with a Bachelors of Arts Degree in Theoretical Physics with a minor in Mathematics. While studying at the University of Tennessee, he was awarded a NIMBioS Assistantship for 2011-2013.